# Microtubule-dependent orchestration of centriole amplification in brain multiciliated cells

Amélie-Rose Boudjema[1]*, Rémi Balagué[1]*, Cayla E Jewett[2], Gina M LoMastro[2,3], Olivier Mercey[4], Adel Al Jord[5,6], Marion Faucourt[1], Alexandre Schaeffer[7,8], Camille Noûs[9], Nathalie Delgehyr[1], Andrew J Holland[2], Nathalie Spassky[1], Alice Meunier[1].

*These authors contributed equally to this work

**Corresponding author:** alice.meunier@ens.fr

1. Institut de Biologie de l'École Normale Supérieure (IBENS), Paris Sciences et Lettres (PSL). Research University, Paris, F-75005, France. CNRS, UMR 8197, Paris, F-75005, France. INSERM, U1024, Paris, F-75005, France
2. Department of Molecular Biology and Genetics, Johns Hopkins University School of Medicine, Baltimore, United States
3. Seagen Inc., Bothell, Washington, United States.
4. Department of Molecular and Cellular Biology, University of Geneva, Geneva, Switzerland
5. Centre for Genomic Regulation (CRG), The Barcelona Institute of Science and Technology, Dr. Aiguader 88, Barcelona 08003, Spain
6. Universitat Pompeu Fabra (UPF), Barcelona, Spain
7. CytoMorpho Lab, Laboratoire de Physiologie Cellulaire & Végétale, Interdisciplinary Research Institute of Grenoble, University of Grenoble-Alpes, CEA, CNRS, INRA, Grenoble France
8. CytoMorpho Lab, UMR8231, ESPCI, University PSL, CEA, Paris France
9. Cogitamus Laboratory, PSL University

# Abstract

Centriole number must be restricted to two in cycling cells to avoid pathological cell divisions. Multiciliated cells (MCC), however, need to produce a hundred or more centrioles to nucleate the same number of motile cilia required for fluid flow circulation. These centrioles are produced by highjacking cell cycle and centriole duplication programs. However, how the MCC progenitor handles such a massive number of centrioles to finally organize them in an apical basal body patch is unclear. Here, using new cellular models and high-resolution imaging techniques, we identify the microtubule network as the bandleader, and show how it orchestrates the process in space and in time. Organized by the pre-existing centrosome at the start of amplification, microtubules build a nest of centriolar components from which procentrioles emerge. When amplification is over, the centrosome's dominance is lost as new centrioles mature and become microtubule nucleators. Microtubules then drag all the centrioles to the nuclear membrane, assist their isotropic perinuclear disengagement and their subsequent collective apical migration. These results reveal that in brain MCC as in cycling cells, the same dynamics -from the centrosome to the cell pole via the nucleus- exists, is the result of a reflexive link between microtubules and the progressive maturation of new centrioles, and participates in the organized reshaping of the entire cytoplasm. On the other hand, new elements described in this work such as microtubule-driven organization of a nest, identification of a spatio-temporal progression of centriole growth and microtubule-assisted disengagement, may shed new light on the centriole duplication program.

**Keywords:** Multiciliated cells, centriole amplification, microtubules, deuterosomes, centrosome, cilia

# Introduction

Centriole amplification is a hallmark of multiciliated cell differentiation necessary for the nucleation of dozens of motile cilia that propel physiological fluids in the brain, the respiratory and the reproductive tracts. It is, however, a pathological mechanism in cancer cells, where it can cause genomic instability that accelerates tumor formation (Nigg & Holland, 2018). Multiciliated cells (MCCs) are post-mitotic, yet increasing evidence suggests that centriole biogenesis during differentiation resembles centriole duplication in cycling cells. First, centriole amplification in MCCs does not require the specialized deuterosome organelles that were thought to be critical for the process (Mercey, Al Jord, et al., 2019; Mercey, Levine, et al., 2019). Second, MCCs co-opt cell cycle and centriole duplication players to control massive centriole production (Al Jord et al., 2017; LoMastro et al., 2022; Revinski et al., 2018; Vladar et al., 2018; Vladar & Stearns, 2007). Thus, understanding the molecular framework driving centriole amplification in MCCs may have implications for both motile ciliopathies and tumorigenesis.

Centriole amplification in MCCs has been described long ago by electron microscopy. More recently, three highly stereotyped sequential phases have been highlighted by live imaging of a GFP-tagged centriole marker in mouse brain MCCs : the amplification phase (called A-stage), during which dozens of latent procentrioles form sequentially around centrosomal centrioles and MCC specific deuterosome organelles; the growth phase (called G-stage), during which all procentrioles elongate synchronously; the disengagement phase (called D-stage), during which all centrioles detach from their growing platforms in a synchronized manner to finally migrate towards the apical membrane and nucleate motile cilia (Al Jord et al., 2014). Since live observations are difficult in respiratory MCCs, the stages of amplification have been finely described by immunostainings (Zhao et al., 2013, 2021). Molecular examination by immunostainings and loss of function experiments on both mouse brain and respiratory MCCs showed that the cell cycle regulators and the centriole duplication molecular cascade used by cycling cells are co-opted in differentiating MCCs to control centriole number, growth and disengagement (Al Jord et al., 2017; Kim et al., 2022; LoMastro et al., 2022; Revinski et al., 2018; Vladar et al., 2018; Vladar & Stearns, 2007).

Despite the similarities between centriole duplication in cycling cells and amplification in MCCs, some aspects of centriole biogenesis remain unexplored in MCCs. In particular, where the massive amount of centrioles emerges in the cell and how they collectively orchestrate their spatial behavior

to finally form an apical basal body patch is unclear. In fact, the huge accumulation of centriole components for massive centriole production, together with the intervention of a poorly characterized deuterosome organelle, complicates the analysis. Some live imaging experiments and electron microscopy suggest that the centrosome could constitute a nest for centriole and deuterosome biogenesis (Al Jord et al., 2014; Kalnins et al., 1972; Mori et al., 2017) but others have proposed that procentriole-loaded deuterosomes emerge independently from the centrosome location, all over the cytoplasm (Nanjundappa et al., 2019; Sorokin, 1968; Zhao et al., 2013, 2019). Interestingly, in the absence of deuterosome, procentrioles are massively amplified from and around centrosomal centrioles, yet, centrosomal centrioles are dispensable (Mercey et al., 2019a; Mercey et al., 2019b; Nanjundappa et al., 2019; Zhao et al., 2019). Finally, in the absence of both centrosomes and deuterosomes, procentrioles are seen emerging from the middle of a self-organized microtubule organizing center (MTOC) suggesting that such MTOC could organize procentriole biogenesis (Mercey et al., 2019). However, pioneer electron microscopy studies on quail oviduct MCC disrupting microtubule function show contradictory results in procentrioles formation and in their subsequent migration (Boisvieux-Ulrich et al., 1987; Boisvieux-Ulrich, Lainé, et al., 1989).

In this context, we developed new tools to resolve the early steps of centriole assembly, and to identify the role of microtubules in the overall amplification orchestration. We used micro-patterned mouse embryonic fibroblasts (MEFs) induced to differentiate into MCCs to impose a reproducible geometry facilitating spatial quantifications. In parallel, we created a knock-in mouse transgenic line co-expressing mRuby-Deup1, the core protein of deuterosomes, and Centrin-GFP, a centriole protein, to document the early dynamics of amplification in brain MCCs. Finally, we performed ultrastructure expansion microscopy (U-ExM) to examine centriole amplification with increased spatial resolution. Together, these analyses (i) characterize the microtubule-dependent formation of a pericentrosomal nest from where procentrioles and deuterosomes emerge, (ii) identify a spatio-temporal pattern of assembly of newborn procentrioles during the amplification (A)-stage, (iii) reveal a subsequent centriole-to-centrosome conversion of procentrioles when arriving at the growth (G)-stage allowing procentrioles to nucleate microtubules and to attach around the nuclear membrane, (iv) show that the subsequent “disengagement” (D)-stage is a combination of deuterosome dismantlement and centriole separation that requires microtubules to proceed, and finally (v) reveal that the collective migration of centrioles to the apical plasma membrane is the result of complex individual motion assisted by microtubules.

# Results

## MEF-MCCs grown on micropatterns localize the onset of centriole amplification at the pericentrosomal region

The origin of amplified centrioles remains controversial partly due to the massive production of small, moving procentrioles within a short period of time. To test if procentrioles are emerging from a particular location in MCCs, we took advantage of a cellular model based on the induced differentiation of MEFs into MCCs by ectopic adenoviral expression of MCIDAS, E2F4 and E2F4 transactivator Dp1 (Kim et al., 2018). This model of MCCs is advantageous because it is not tissue-specific and does not require epithelial cell-to-cell contact for differentiation. This allows single cells to differentiate on micropatterns that impose a reproducible cytoplasmic organization facilitating spatial quantifications. We induced MCC differentiation in MEFs grown on crossbow-shaped micropatterns to analyze the global spatial dynamics of procentriole amplification (Fig. 1A). We first confirmed that, in MEF-MCCs, the same dynamics of amplification was observed as in brain MCC: an “amplification stage (A-stage)”, marked by the progressive accumulation of immature non-polyglutamylated procentrioles is followed by a “growth stage (G-stage)” where procentrioles mature and become polyglutamylated. This maturation is followed by ciliation which is often partial, probably because of the absence of the typical epithelial apico-basal polarity (Fig. 1B). Consistently, in this cellular model, centrosomes can localize below the nucleus. Here, only cells with apically positioned centrosome were studied. By density mapping the location of apical centrosomes in multiple crossbow-shaped MEFs, we confirmed that they are located at a reproducible location and at the center of convergence of microtubules (Fig. 1C, top row left) where a pericentrin (PCNT) cloud is organized (Fig 1D, top row left). Then, by density mapping the position of SAS6+ procentrioles in multiple differentiating MEF-MCCs containing less than 10 SAS6 foci (early A-stage), we observed that early procentriole emergence is localized in this centrosomal region, where PCNT also accumulates (Fig. 1C, 1D top row middle). Later during amplification (>10 SAS6+ foci, late A-stage and G-stage), procentrioles occupy a larger portion of the cells centered around the centrosome location and surrounding the nuclear region (Fig. 1C top row right). By contrast, PCNT stays concentrated in the centrosomal region (Fig. 1D top row, right).

We previously showed in brain MCC deprived of both centrosomes and deuterosomes, that centrioles emerged from the center of a self-organized microtubule network emerging from a PCNT cloud. To test whether microtubules drive the organization of a centrosomal nest from which

procentrioles emerge, we treated MEF-MCCs with nocodazole before the onset of centriole amplification. In this condition, SAS6+ structure density mapping shows a clear dispersion of early procentrioles compared to control cells where they focalize in the pericentrosomal region (Fig. 1C bottom row). The centrosomal PCNT cloud also scatters in the cell cytoplasm (Fig. 1D bottom row). Since MT perturbation also induced centrosomal centriole splitting and decentralization of centrosomal centrioles (Fig. 1C, bottom row left; Fig. 1 Supplementary 1A), we also measured the distance between emerging SAS6+ foci and the closest centrosomal centriole. This showed that procentriole to centrosome distance increases with nocodazole (Fig. 1 Supplementary 1A-B).

Altogether, these results suggest that, in this non tissue specific proxy of MCC progenitors, microtubules organize the onset centriole amplification in the pericentrosomal region.

## Deup1 is a centrosomal protein and assembles deuterosomes in the pericentrosomal region in brain MCC

We then sought to study centriole amplification onset in physiological MCCs. Live monitoring of centriole amplification in physiological MCCs has been done only in brain MCCs since respiratory and reproductive MCCs are part of stratified epithelia, hindering their live observation by high-resolution live-cell microscopy. In brain MCCs, centriole amplification has been previously monitored using GFP-tagged Centrin2 but these experiments could not resolve the early events of amplification due to Centrin accumulation in the pericentriolar material (PCM) in addition to its integration in nascent procentrioles. To highlight the dynamics of early centriole amplification in MCCs, we developed a transgenic mouse line expressing Centrin2-GFP (Cen2-GFP), together with the core deuterosome component Deup1, endogenously tagged with a mRuby fluorescent reporter (mRuby-Deup1; Fig. 2A). Live imaging cells from these animals allow to monitor the dynamics of endogenous Deup1 structures during the A-, G- and D-stages, detectable using Cen2-GFP (Fig. 2B).

To monitor what occurs before, or at the very beginning of A-stage, we live imaged early cultures of Cen2-GFP; mRuby-Deup1 MCC progenitors. This revealed that Deup1 accumulates as a cloud around the centrosome in 100% of the analyzed MCC progenitor (Fig. 2C, 00:00 to 05:00; Video 1, n=12 cells), before the onset of A-stage where the first procentrioles, taking the form of Cen2-GFP+ “halos” around a mRuby-Deup1+ structure, are observed (Fig. 2C, from 07:00, arrows). To characterize this early stage, we increased the spatial resolution on early amplifying cells and identified the “cloud” as composed of foci of Deup1 and Centrin that are often in close proximity but not necessarily colocalized (Fig. 2D). Live imaging notably shows that Deup1 and

Centrin move independently from each other (Fig. 2D; Video 2). Increasing temporal resolution to 5-15s reveals that Deup1+ foci observe an oscillatory dynamics to the centrosome (Fig. 2E, colored arrows, Video 3, 5/10 cells observed for 1-4min). This oscillating movement to the centrosome is reminiscent of the dynamics of the centriolar satellite protein PCM1 in *Xenopus* and mice, and the PCM protein Centrosomin in *Drosophila* (Hall et al., 2023; Kubo et al., 1999; Megraw et al., 2002), suggesting that Deup1 is a centrosome-related protein with similar dynamics to other pericentrosomal components. Interestingly, during this dynamic movement, Deup1 aggregates can connect and disconnect with one centrosomal centriole (Fig. 2F; Video 4) or can stay connected for hours (Fig. 2D), maybe explaining the previously described preferential localization of Deup1 with the centrosomal daughter centriole (Al Jord et al., 2014; Mercey et al., 2019; Mercey et al., 2019).

Over time, Deup1 foci within the cloud become more spherical, associate with Cen2 signal and begin to exit the cloud (Fig. 2C, 07:00 and 09:00), marking what we previously described as A-stage (Al Jord et al., 2014, 2017). Live imaging with increased spatial and temporal resolution shows that A-stage loaded deuterosomes have comparable back-and-forth movement toward the centrosomal cloud as Deup1 foci during the cloud stage (Fig. 2G, white arrows; Video 5, 13/15 cells observed for 1-4min) until deuterosomes move away from the centrosomal cloud and from each other (Fig. 2G, blue arrows, Fig 2C, 07:00-12:00).

Altogether these data show that centriole amplification emerges in the centrosomal region by the accumulation of a cloud of Centrin and Deup1 foci. Deup1 oscillatory dynamics is reminiscent to other centrosome-related proteins. After expansion of this cloud, deuterosomes loaded with A-stage Cen2-GFP+ procentrioles exit the cloud, while maintaining centrosome-centered oscillating dynamics. This oscillatory behavior suggests a physical link between Deup1 structures and the centrosome.

## Procentriole assembly begins in a pericentrosomal nest and continues during radial migration

To better resolve the very early steps of centriole assembly within the identified pericentrosomal nest, we increased spatial and molecular precision by performing ultrastructure expansion microscopy (U-ExM) on early amplifying cells. U-ExM is an extension of expansion microscopy that allows the visualization of structures by optical microscopy with 4-fold increased resolution (Gambarotto et al., 2019).

U-ExM analysis reveals that the cloud of centrin and Deup1, characterized by live imaging, precedes the onset of centriole biogenesis. In these fixed detergent-treated cells, the cloud is around

10-fold dimmer than the centrosomal centrioles, and thus difficult to visualize without over-saturating the signal (Fig. 3 Supplementary 1). More precisely, U-ExM observations suggest that centrin accumulates in a cloud around parent centrioles prior to Deup1 (Fig. 3 Supplementary 2A). Next, Deup1 forms foci at and around the parent centrioles (Fig. 3A, Fig. 3 Supplementary 2B). This cloud of Deup1 and Centrin also includes PCNT (Fig. 3 Supplementary 2C). Notably, centrin and Deup1 foci are often in close proximity but not colocalized, confirming live imaging, while PCNT puncta partially overlap with centrin (Fig. 3 Supplementary 2C). At this stage, PLK4, the master regulatory kinase, and SAS6, one of the first centriolar components are either absent, or present as small foci within the cloud, often on the wall of the parent centrioles (Fig. 3B-C).

As Deup1 accumulates, the foci within the cloud become more regular in shape and colocalize with PLK4 and SAS6 which mark the formation of nascent procentrioles on Deup1 structures, and the beginning of A-stage. These procentrioles are however deprived of β-tubulin and therefore of a microtubule wall (Fig. 3D-F). At this stage, it is unclear whether the Deup1 foci growing these nascent procentrioles are bona fide electron dense spherical deuterosomes. Since these nascent procentrioles are deprived of microtubules, it hinders the detection of this stage by EM studies. As the number of nascent procentrioles increases, they migrate away from the centrosome and β-tubulin is recruited asynchronously on procentrioles, with procentrioles further away from the parents acquiring tubulin, and procentrioles closer to the parents often lacking tubulin (Fig. 3G-K, Fig. 3 Supplementary 2D). At this stage the circular organization of multiple procentrioles confirm the deuterosome identity of the central Deup1 structure. Consistent with a progression of procentriole assembly during radial migration, the procentriole walls increase in length from 90nm to 170nm and in width from 110nm to 220nm as a function of distance from the parent centrioles (Fig. 3L-M and Fig. 3 Supplementary 2D). These sizes are greater than the ones measured during “halo” A-stage in our previous study by electron microscopy, probably because of light diffusion (Al Jord et al., 2014). Around the same time as tubulin, centrin is also recruited to procentrioles (Fig. 3I). This stage is probably the stage that we previously documented as A-stage by Cen2-GFP live imaging and correlative Cen2-GFP/EM microscopy. Centriolar microtubules are then acetylated on procentrioles migrating away from the parents (Fig. 3I). The Deup1 asymmetry previously described at the centrosomal daughter centriole (Al Jord et al., 2014) becomes visible in some cells during the cloud stage (Fig. 3B, N; Fig. 3 Supplementary 2B) and in a majority of cells during A-stage (Fig. 3F-H, N), while procentrioles achieve their final width and length during G- and D-stage (Fig. 3 Supplementary 2 D-H).

Altogether these data reveal that (i) a pericentrosomal nest composed of centrin, PCNT and Deup1 is preassembled before the onset of centriole amplification, (ii) centriole biogenesis begins in this nest before what had been previously resolved using Cen2-GFP and EM (iii) the first steps

involve the formation of procentrioles deprived of their microtubule wall, (iv) which is followed by the recruitment of microtubules, that undergo progressive growth and acetylation during the radial migration of deuterosomes away from the nest (summarized in Fig. 3O-P).

## Microtubules organize the pericentrosomal nest, promote deuterosome formation and hinder deuterosome dispersion

MEF-MCCs experiments suggest that the pericentrosomal nest is organized by microtubules (Fig. 1 C-D). Fine microtubule organization during the different steps of centriole amplification has never been described in MCC. Using tyrosinated tubulin antibody to stain for the dynamic microtubule population in brain MCC progenitors, we observed that microtubules are typically focalized to the centrosome before and during A-stage (Fig. 4A). This polarity is progressively lost during the following G- and D-stages. Finally, at the end of amplification, when centrioles become basal bodies nucleating cilia, microtubules repolarize from the basal body patch, consistent with the known role of basal bodies having acquired a basal foot as microtubule organizing center in terminal MCC (Herawati et al., 2016; Kunimoto et al., 2012; Z. Liu et al., 2020; Tateishi et al., 2017) (Fig. 4A). To further characterize the role of microtubules in the dynamics of centriole amplification, we set up nocodazole treatment protocols to perturb the microtubule network while allowing for the progression of centriole amplification in brain MCC cultures (Fig. 4 supplementary 1A-B).

Then, we live imaged Cen2-GFP; mRuby-Deup1 brain MCCs during cloud or early A-stage after acute addition of nocodazole (10µM, added after the first time point). We observed that in the DMSO condition, the Deup1+ cloud forms, expands, and when deuterosomes loaded with Cen2-GFP+ procentrioles are released from the cloud, they remain in the cloud periphery covering a mean surface of 36µm$^2$ +/-9,3µm$^2$ (Fig. 4B-D, Video 6). By contrast, under nocodazole treatment, the formation of the Deup1+ centrosomal cloud is hindered or the Deup1+ cloud is dissolved when already present (Fig. 4B-C; Video 6). In addition, Deup1 foci/deuterosomes appear scattered all over the cytoplasm, instead of the pericentrosomal region, frequently covering the entire cell surface (123µm$^2$ +/- 63,1µm$^2$; Fig. 4B, D; Video 6). Immunostainings combined with super-resolution confocal microscopy show that the Deup1 structures formed in these conditions are, in fact, a group of small deuterosomes, each loaded with a single procentriole (Fig. 4E). Consistent with a scattered apparition of deuterosomes, immunostainings of A-stage cells after such treatment showed that the centrosomal cloud of PCNT disappears, leaving PCNT only at centrosomal centrioles and procentrioles (Fig. 4 Supplementary 1C). To determine whether the oscillations of

Deup1 foci to and from the centrosome during the cloud stage, and of deuterosomes during A-stage, are microtubule-dependent, we increased the temporal resolution to dt=15s after acute nocodazole treatment. We found that oscillations of both types of Deup1+ structures nearly disappear in nocodazole-treated cells (Fig. 4F). Altogether, this shows that microtubules organize the centrosome nest and the focalized emergence of capacious procentriole-loaded deuterosomes. They also retain the deuterosomes in an area around the centrosome, through an oscillatory dynamics, preventing their dispersion throughout the cell.

To analyze the consequences of a full differentiation under nocodazole and further assess how microtubule perturbation affect centriole amplification, we treated cells chronically for 48h with nocodazole (1 and 5µM) from the onset of differentiation. First, the number of SAS6+ cells appearing in the culture slightly decreased suggesting that microtubules may help the cells to begin centriole amplification (Fig. 4 Supplementary 1D). Next, we analyzed cells able to amplify centrioles and analyzed SAS6+ loaded deuterosomes during G-stage, when the final number of deuterosome is reached (Mercey, Al Jord, et al., 2019). Consistent with what was observed during acute treatment, we observed that in nocodazole treated cells, deuterosomes are more numerous but smaller and loaded with fewer centrioles than in the control (Fig. 4G-H). As a result, we observed a slight decrease in the number of procentrioles produced in these cells during G- and D-stage (Fig. 4J).

Altogether, these data show that microtubules organize the centrosome nest from which procentriole-loaded deuterosomes emerge and keep them in a restricted area around the centrosome during A-phase, through typical centrosomal oscillations. In addition to dispersal of deuterosomes, microtubule perturbation leads to the formation of small and scarcely loaded deuterosomes suggesting that focalization of deuterosome/centriole components is required for the formation of capacious deuterosomes. This focalization may enhance the efficiency of centriole production since the number of cells amplifying centrioles and the number of procentrioles produced in these cells are slightly decreased when microtubules are depolymerized.

## Procentrioles convert to multiple microtubule organizing centers (MTOC) at the growth phase (G) transition

We then set out to study the role of microtubules when all procentrioles have been produced, after A-phase completion. First, we needed to identify which structure(s) was organizing microtubules as microtubule polarization to the centrosome is lost from G-stage (Fig. 4A). We hypothesized that procentrioles produced during A-stage may have converted into microtubule-

organizing centers (MTOC) during the maturation process occurring during G-stage (Al Jord et al., 2014), multiplying the sources of microtubule nucleation. Such “centriole-to-centrosome” conversion occurs in cycling cells at the G2-M transition, is Plk1 dependent and is achieved through the acquisition of the pericentriolar material (PCM) (Joukov & De Nicolo, 2018). In MCCs, the A-to-G transition shares molecular similarities with the G2-to-M transition and is Plk1 dependent (Al Jord et al., 2014, 2017). We stained brain MCC progenitors for Plk1 and PCNT, a core PCM protein. This showed that Plk1 appears at procentrioles during the A-to-G transition (Fig. 5B, 5D) and that G-stage procentrioles recruit significantly more PCNT than A-stage procentrioles (Fig. 5A, 5C). The same observation is made on Deup1 KO cells showing that the procentrioles recruit this PCM protein (Fig. 5 Supplementary 1A). However, PCNT recruitment was greater in WT procentrioles compared to Deup1 KO cells (compare Fig. 5C to Fig. 5 Supplementary 1A) suggesting that deuterosomes may also participate in PCNT recruitment. Consistent with Plk1 and PCNT recruitment, microtubule regrowth experiments in both MEF-induced and brain MCCs showed that GT335 positive G-stage procentrioles display a microtubule regrowth efficiency significantly greater than GT335 negative A-phase procentrioles, which are often barely able to regrow microtubules (Fig. 5E-H). Altogether, this reveals that, from the G-stage, tens of centrosome-like structures are present in MCC progenitors, participating in microtubule cytoskeleton organization.

## Microtubules attach procentrioles to the nuclear membrane and are required for subsequent disengagement

The A-to-G transition is marked by the migration of the centriole-loaded deuterosomes to the nuclear membrane and their perinuclear distribution (Fig. 6A 00:00, videos 7, Fig. 6 Supplementary 1A, Video 8) (Al Jord et al., 2017). We sought to test whether microtubules nucleated by G-stage procentrioles were involved in this perinuclear migration and distribution. In fact, this dynamics is reminiscent of the centrosome migration that occurs during the G2-to-M progression in cycling cells in preparation for mitotic spindle organization. In cycling cells, this migration is driven by molecular motors attached to nuclear pores, pulling the microtubules nucleated by the two centrosomes (Agircan et al., 2014). First, time-lapse experiments allowing single deuterosome tracking showed that, once in contact, procentrioles remain adjacent to the nuclear periphery where they can migrate along the nuclear membrane for several hours until they disengage (Fig. 6B-C, video 9). In addition, co-staining of centrioles and nuclear pore proteins show a tight colocalization (Fig. 6 Supplementary 1B). Then, brain MCC progenitors acutely treated with

nocodazole (10µM, 4h) showed a drastic decrease in the proportion of G-stage centriole-loaded deuterosomes localized at the nuclear membrane (Fig. 6D-F). Finally, nocodazole (10µM) treatment on live-imaged cells where procentriole-loaded deuterosomes have already migrated to the nuclear membrane, shows detachment of procentrioles from the nucleus within minutes, showing that, not only migration, but also attachment of procentrioles to the nuclear membrane is microtubule dependent (Fig. 6 Supplementary 1C, video 10).

We then wondered whether this microtubule dependent dynamics was required for an efficient subsequent centriole disengagement during the following D-stage. We first described with high spatial and temporal resolution the relationship between disengaging procentrioles and the nuclear membrane. At the single deuterosome resolution, we could score that nearly all G-phase procentrioles contacted the nuclear membrane before flower dismantlement (Fig. 6G). Then, monitoring tens of disengagement movies, we identified a transient stage during which disengaging procentrioles redistribute isotropically in the 3 dimensions, along the nuclear membrane (Fig. 6A, 4:30, Video 7) before losing its contact to migrate to the apical surface (Fig. 6A, 6:30 to 14:00). This can be observed even in cells where deuterosomes are not evenly distributed around the nucleus before disengagement and therefore reveals that during the individualization process, centrioles are not only attached, but pulled away from each other. Finally, confirming centriole attachment during disengagement, acute nocodazole 10µM treatment on D-stage cells leads to the immediate release of disengaging procentrioles from the nuclear membrane (Fig. 6 Supplementary 1D, Video 11).

We and others previously showed that centriole disengagement in MCC progenitors is dependent on Plk1, APC/C and separase activity like in cycling cells (Al Jord et al., 2017; Revinski et al., 2018). Our data now suggest that this process could be assisted mechanically by MTs. To test this, we chronically treated brain MCCs with increasing doses of nocodazole (1-5µM, 48h) and analyzed whether procentrioles were able to individualize. We observed that at low doses, the proportion of cells in “D-stage” remained unchanged, but significantly more “D”-stage cells showed incomplete disengagement compared to controls (Fig. 6H-J). Interestingly, within those with incomplete disengagement, we often saw SAS6 negative procentrioles still engaged to deuterosomes, a phenotype rarely observed in controls (Fig. 6 Supplementary 1E-F, white arrows). Indeed, SAS6 normally disappears from procentrioles when centrioles are docked, just before ciliation (Al Jord et al., 2014). This suggests that centrioles were able to degrade SAS6, a process also dependent on APC/C (Strnad et al., 2007), but failed to disengage from deuterosomes. Then, with higher dose of nocodazole, “D”-stage cells are rarely observed (Fig. 6I). These observations under chronic nocodazole treatments suggest that microtubules are involved in efficient centriole disengagement. To confirm, we performed acute nocodazole (10µM) treatment on G-stage cells and

observed in live that the detachment of centriole-loaded deuterosomes from the nuclear membrane is accompanied by a long, unsynchronized and sometimes incomplete disengagement (Fig. 6K-L, Video 12).

Altogether these data suggest that the acquired ability of the newly formed centrioles to nucleate microtubules at the A-to-G transition, drive their nuclear attachment and assist their subsequent disengagement.

## Disengagement of centrioles is a combination of centriole separation from deuterosomes, deuterosome splitting and dissolution

Contrary to A-stage which can take up to 20 hours, D-stage can proceed in less than an hour and typically takes around 3 hours (Al Jord et al., 2017). Dynamics of disengagement has previously been described using Cen2-GFP expressing cells, where disengagement takes the form of the dismantlement of empty flower-like structures, representing Cen2-GFP+ procentrioles organized around deuterosomes ("deuterosome pathway"; Fig. 6A), as well as disengagement of procentrioles that grow from the centrosomal centrioles ("centriolar pathway"; plain flower-like structures, arrows; Fig. 6A). To characterize the dynamics of centriole disengagement from deuterosome structures, we used the Cen2-GFP; mRuby-Deup1 transgenic line and observed that the dismantlement of Cen2-GFP+ flowers results from the combination of 3 different processes that occur concomitantly (Fig. 7A, Video 13). First, individual procentrioles negative for mRuby-Deup1 appear in the cell during the disengagement process suggesting that they can detach from Deup1 structures (Fig. 7A; 00:00, white arrows). Second, over the course of disengagement, single cell analysis shows a decrease in deuterosome size correlated with an increase in the deuterosome number, suggesting that deuterosomes split (Fig. 7B-C). Splitting of deuterosomes can give rise to single centrioles with a Deup1+ proximal end, showing that centrioles can also individualize from deuterosomes through the dismantlement of the deuterosome structures (Fig. 7A; 01:40, red arrows). Third, a general disintegration of Deup1 occurs as disengagement progresses, giving rise to Deup1 foci that spread all over the cytoplasm, contrasting with the focalized centrosomal Deup1 cloud observed at the beginning of amplification (Fig. 7A, mRuby-Deup1 diffuse signal at 4:10). Consistent with a disengagement assisted by mechanical forces, individualized procentrioles can be seen migrating away from each other, along the nuclear periphery (Fig. 7D; Video 14; Fig. 7 Supplementary 1A and Video 15) and located within MT nodes (Fig. 7E; Video 16). At the end of disengagement, centriole-free and dense Deup1 aggregates can remain for hours after centriole disengagement, before finally disappearing after ciliation (Fig. 7 Supplementary 1B). This is

consistent with the “late deuterosomes” described by electron microscopy (Guirao et al., 2010). In line with our live imaging observations, and consistent with what was described in respiratory cells (Zhao et al., 2013), U-ExM of D-stage cells show the co-existence of small deuterosomes with single procentrioles, procentrioles without Deup1 and centriole-free deuterosomes along the nuclear membrane (compare Fig. 7F and 7G). Some centriole-free deuterosomes can persist in the apical portion of the cell until after ciliation (Fig. 7 Supplementary 1C).

Altogether, these results show that disengagement consists of centriole detachment from deuterosomes, deuterosome splitting and Deup1 disintegration. Since this process is microtubule-dependent and occurs from structures that are dragged along the nuclear membrane, this suggests that mechanical forces induced by microtubules between the nuclear membrane and centrioles contribute to centriole/deuterosome separation and deuterosome dismemberment.

## Disengaged centrioles finally converge apically with the former centrosome in a microtubule-dependent manner

After disengaging, centrioles detach from the nuclear membrane (Fig. 6A; 06:30) and migrate from all over the nucleus to the apical cell surface (Fig. 6A; 06:30-14:00) to dock and nucleate motile cilia (Boisvieux-Ulrich et al., 1987, 1990; Boisvieux-Ulrich et al., 1989). This is followed by an acto-myosin dependent planar basal body constriction (Hirota et al., 2010). Dynamics of this collective migration process has never been analyzed and is tedious since MCCs produce several dozens of centrioles that are therefore difficult to track. To begin, we first analyzed the global 3D displacement of all centrioles in individual cells, by segmenting the Cen2-GFP signal throughout their apical migration over time-lapse imaging. As a cellular reference, we took one of the centrosomal centrioles, trackable using their higher Cen2-GFP fluorescence, in cells where the 2 centrosomal centrioles stay close together. This global quantification showed that, at the end of disengagement, centrioles are evenly distributed within a mean radius of 8µm with respect to the tracked centrosomal centriole (in the range of the nucleus radius). Then, by the end of apical migration and basal body constriction, centrioles are predominantly (65%) located in a radius of 3µm around this reference point (Fig. 8A). This significant histogram shift ($Chi^2$ test, $p<0.0001$) suggests a collective movement of newly formed centrioles that bridges them together and with the centrosomal centrioles. Consistently, centrosomal centrioles finally dock within the newly formed basal body patch and also nucleate cilia (Z. Liu et al., 2020).

To then analyze the displacement dynamics of individual centrioles, we performed live imaging with high temporal resolution (dt=5min) over the entire migration process. This allowed us

to manually track a subset of migrating centrioles and catch their individual trajectories before they reach the group (Fig. 8B, Video 17). Single centrioles move at 0,12+/-0,09µm/min. Consistent with the global 3D gathering of the whole centriole population, they are seen converging apically toward the centrosomal centriole reference point as reflected by the time-correlated decrease of their distance and by the mean vector directionalities of individual trajectories (Fig. 8B-C, Video 17). Although single centrioles display a global directional migration, analysis of the shape of the trajectories, speed of displacement and directionality with regard to the centrosome reference point, show that their migration is marked by back-and-forth movements oscillating between diffusive and more processive steps (Fig. 8D, Fig. 8 Supplementary 1A). As steps toward the centrosome are more numerous and more rapid than steps away (Fig. 8 Supplementary 1B), centrioles finally slowly converge at 0,01+/-0,03um/min. Interestingly, within this complex behavior, the z-motion, when centrioles below the nucleus migrate up around the nuclear membrane (Fig. 8B; light blue, dark blue and red trajectories), is clearly processive toward the apical pole, (Fig. 8D, light blue dots; Fig. 8E) and more rapid (Fig. 8F, Fig. 8 Supplementary 1C) than the steps in the XY plane .

To define the involvement of microtubules in this collective migration process we acutely treated cells with nocodazole (10µM) at the G-to-D transition (Fig. 8G). As expected, centrioles immediately detach from the nuclear membrane and scatter away (Fig. 6 Supplementary 1D). Their subsequent movements appear more erratic with centrioles migrating away from the initial position of the centrosome, and groups of centrioles migrating up and down the nucleus (Fig. 8H; Video 18). Consistent with the apparent erratic individual movement, global migration of centrioles to the apical side of the cell took longer in nocodazole treated cells, and can remain incomplete during the course of 20h live imaging experiments (Fig. 8I). In fixed samples, chronic nocodazole treatments (48h, 1-5uM) suggested that centrioles finally succeed in migrating up (Fig. 8 Supplementary 1D) but not in gathering accurately in the XY plane, as revealed by the wider surface covered by the basal body patch (Fig. 8J; Fig. 8 Supplementary 1E).

Altogether, these data show that centrioles migrate collectively, following a complex and slow motion, from all over the nuclear membrane, to gather with the former centrosome. The migration is characterized by oscillations between forward and backward directionalities and between processive and diffusive movements, but switches to a more processive and rapid motion when directed toward the apical pole. Centriole movements are affected when microtubules are altered and consequently, the migration is perturbed in the 3 dimensions.

# Discussion

Since pioneer electron microscopy studies on basal body production in quail oviduct MCC 35 years ago (Boisvieux-Ulrich et al., 1987, 1990; Boisvieux-Ulrich et al., 1989), this work is the first to assess the role microtubules in the now finely described centriole amplification process. This lack is probably due to the difficulty of developing a protocol that allows each microtubule-dependent step to be observed separately. Taking advantage of our live imaging assay and newly developed cellular models, our work identifies a reflexive link between microtubules organization and centriole amplification where microtubules are first organized by the former centrosome, where they organize a nest for procentrioles production, and then by the maturing centrioles where they assist their perinuclear organization, disengagement and final apical migration for cilia nucleation.

Using live imaging on brain MCC, we highlight the existence of a nest composed of Deup1, PCNT and Centrin2, pre-assembled before the amplification onset. Procentriole-loaded deuterosomes are seen emerging from this nest. Both formation of the nest and focalized emergence of deuterosomes are perturbed when microtubules are depolymerized, leading to the formation of small and scarcely loaded deuterosomes. These observations suggest that microtubules, organized by the centrosome, concentrate deuterosome and centriole components to optimize amplification. Whether this concentration of proteins results from the retrograde transport of the proteins themselves, as suggested by the microtubule dependent oscillatory dynamics of Deup1 foci to the centrosome, or of their mRNA through centrosomally concentrated centriolar satellites (H. Liu et al., 2023; Odabasi et al., 2019), need further investigations. Consistent with the existence of this nest, in the absence of deuterosomes in Deup1 KO MCC, amplified centrioles are emerging on, and around, the centrosomal centrioles (Mercey et al., 2019) and when both centrosome and deuterosomes are absent, procentrioles emerge in a cloud of PCM, at the convergence of the microtubule network (Mercey et al., 2019).

Whether the existence of such a pericentrosomal nest exists in respiratory and reproductive cells is unclear. Live imaging is difficult to perform because cells are in a stratified epithelium. In addition, the number of centrioles produced is much greater than in brain cells, albeit very rapidly. Consequently, the early dynamics of amplification is difficult to describe. However some studies in fixed cells at early stages proposed a pericentrosomal onset of procentrioles and deuterosomes emergence in chick and mouse airway MCCs (Al Jord et al., 2014; Kalnins et al., 1972; Mori et al., 2017). Also, our observations in non-tissue specific MEF-MCCs suggest that, at least the onset of amplification, occurs in a pericentrosomal nest. However, in a context of massive centriole production, the concentration of centriole components may reach the threshold for centriole biogenesis in the nest first, and then in the rest of the cytoplasm.

Using U-ExM, we further reveal a radial progression of centriole biogenesis from the pericentrosomal nest. Our static observations suggest that (i) Plk4 and SAS6 first accumulate at the parent centrioles and inside the nest, (ii) nascent SAS6+ procentrioles deprived of a microtubule wall appear on small Deup1+ structures, and then (iii) procentrioles acquire a growing and acetylating microtubule wall while radially migrating away from the nest. This spatio-temporal progression of centriole biogenesis supports the sequential emergence of procentrioles in the centrosomal region and is consistent with theoretical modeling, simulations and *ex cellulo* experiments suggesting that the place where a critical threshold level of Plk4 activation is surpassed determines procentrioles' apparition spot (Nabais et al., 2021). Preferential Deup1 accumulation to the daughter centriole previously described (Al Jord et al., 2014; Mercey et al., 2019 a&b) was shown here to appear from the cloud stage, and to become prominent during A-stage. Live experiments highlight oscillations of Deup1, comparable to PCM1 oscillations (Hall et al., 2023), leading to Deup1 association and dissociation from a centrosomal centriole. Since PCM1 was also shown to accumulate asymmetrically to the daughter centriole, this suggests a preferential route/affinity for pericentrosomal proteins to the immature centrosomal centriole (Tozer et al., 2017).

This study also reveals that Deup1 -the core component of deuterosomes (Zhao et al., 2013)- is a centrosomal protein before building deuterosome structures, supporting their denomination as centrosome auxiliaries (*deuter* "second" and *soma* 'body). Sorokin in 1968, who named deuterosomes, was speaking about solid crystallization of a super-saturated solution of deuterosome components (Sorokin, 1968). Yet, increasing evidence shows that liquid-liquid phase separation is a prominent mechanism involved in the formation of spherical non membranous organelles. Recently, formation of Deup1 pure condensates in solution as well as FRAP experiments after overexpression of Deup1 in MCC progenitors suggested that deuterosomes where not liquid-like structures (Yamamoto & Kitagawa, 2019). Consistently, we never observed fusion events of Deup1 condensates in our time lapse experiments. More importantly, we did FRAP experiments on endogenously tagged mRuby-Deup1 in cells at the different stages of centriole amplification, and did not find significant recovery, supporting that centrosomal Deup1+ foci and deuterosomes are not liquid like structures (Fig. 8 Supplementary 2).

We also finely describe the spatial switch in procentriole organization occurring around the A-to-G transition, where the focalized emergence of procentriole-loaded deuterosomes characteristic of early A-stage is followed by their migration and distribution around the nuclear membrane by G-stage. We further show that this transition (i) is correlated with the maturation of procentrioles, marked by the accumulation of PCNT, the recruitment of Plk1 and the acquisition of their ability to nucleate microtubules and (ii) is microtubule dependent. This reminds the centriole-

to-centrosome conversion occurring at the G2-M transition followed by the associated microtubule dependent nuclear migration of new centrosomes at mitosis onset (Agircan et al., 2014). Since both transitions are regulated by Plk1 and Cdk1, it's very likely that the same mechanisms are at work in both cycling cells and brain MCC.

Most surprisingly, centriole disengagement, which is known to be Plk1 and APC/C dependent (Al Jord et al., 2017; Kim et al., 2022; Ruiz García et al., 2019), is tightly correlated with this nuclear association. First, the migration of procentriole loaded deuterosomes systematically precedes centriole disengagement. Second, disengagement proceeds through centriole separation from deuterosomes and deuterosome splitting along the nuclear membrane. Third, disengagement is followed by the migration of individualized procentrioles along the nuclear membrane. Finally, microtubule depolymerisation detaches disengaging centrioles from the nucleus and hinders centriole disengagement. Altogether this strongly suggests that mechanical forces pulling procentrioles to the nuclear membrane, assist centriole disengagement. One could therefore hypothesize that, once the molecular switch of the mitotic oscillator is 'on', the splitting and/or separation of deuterosomes and centrioles require microtubule driven mechanical forces to proceed. It would be interesting to test whether, in cycling cells, centriole disengagement is also assisted by forces exerted by microtubules nucleated by the maturing daughter centriole.

Disengagement around the nuclear membrane is followed by the migration of centrioles to the apical cortex to dock and nucleate cilia. Characterizing this process has never been done and is very challenging since individual centrioles move in close proximity with tens of other centrioles. Following individual trajectories requires high resolutive spatio-temporal live imaging while avoiding excessive light exposure which disturbs centriole migration (Boudjema et al., 2024). Our trackings reveal a global apical convergence of new centrioles around the former centrosome. Using high temporal resolution microscopy, we further identify that individual dynamics is complex and can be splitted between the baso-apical migration, where centrioles move in a processive and more rapid way around the nuclear membrane to reach the centriole patch, and the apical motion, marked by alternance between back and forth movements and between diffusive and more processive steps. Such intermittent movement is probably multifactorial. It may result from the resistance of a crowded environment on a massive population of large organelles that congregate (Vale, 1985), to the binding and release of centrioles by molecular motors (Ananthanarayanan et al., 2013), to a combined action of microtubules with the acto-myosin network which is known to be concentrated apically in terminally differentiated MCC (Kunimoto et al., 2012; Lemullois et al., 1988; Sedzinski et al., 2017), and to an asynchronized docking of centrioles.

The rate of migration is in the range of microtubule dependent centriole migration in mouse olfactory neurons (Ching et al., 2022) and in the dendrite of *C. elegans* sensory neurons (Li et al.,

2017). If we follow the parallel existing between centriole amplification and centriole duplication in cycling cells (Al Jord et al., 2017), this migration stage may be compared to mitosis with a high number of centrosome-like structures. Consistently, when the mitotic oscillator is dis-inhibited and cells enter pseudo-mitotic events, centrioles show clear and rapid cell-cycle like clustering (Al Jord et al., 2017). One could therefore hypothesize that centriole convergence in MCCs is driven by the same mechanisms as the clustering events described in cycling cells with amplified centrosomes (Kalkan et al., 2022; Marthiens et al., 2012). Consistent with a combined role of microtubule and actin proposed in centrosome clustering for mitosis, migration for primary ciliogenesis (Pitaval et al., 2017) as well as basal body migration for motile ciliogenesis in old electron microscopy studies (Boisvieux-Ulrich et al., 1990; Boisvieux-Ulrich et al., 1989), the migration can proceed, albeit incompletely, in the presence of nocodazole.

Altogether, this study shows that the microtubule cytoskeleton shapes, and is shaped, by centriole amplification in brain MCCs (Fig. 9). It further strengthens the parallel between MCC differentiation and the cell cycle. In both cases, the co-existence of two generations of centrioles, together with their step-wise maturation, shape the spatio-temporal organization of an intracellular process. On the other hand, new features described in these post-mitotic cells such as microtubule-driven organization of a centriole biogenesis nest, the radial progression of centriole formation and microtubule-assisted disengagement, may shed new light on the centriole duplication program.

**See supplementary materials for methods, 9 supplementary figures and their captions and 18 movie captions. Video files are available on: https://doi.org/10.5281/zenodo.10589876.**

# References


Agircan, F. G., Schiebel, E., & Mardin, B. R. (2014). Separate to operate: Control of centrosome positioning and separation. *Philosophical Transactions of the Royal Society B: Biological Sciences*, *369*(1650), 20130461. https://doi.org/10.1098/rstb.2013.0461

Al Jord, A., Lemaître, A.-I., Delgehyr, N., Faucourt, M., Spassky, N., & Meunier, A. (2014). Centriole amplification by mother and daughter centrioles differs in multiciliated cells. *Nature*, *516*(7529), 104-107. https://doi.org/10.1038/nature13770

Al Jord, A., Shihavuddin, A., Servignat d'Aout, R., Faucourt, M., Genovesio, A., Karaiskou, A., Sobczak-Thépot, J., Spassky, N., & Meunier, A. (2017). Calibrated mitotic oscillator drives motile ciliogenesis. *Science*, *358*(6364), 803-806. https://doi.org/10.1126/science.aan8311

Ananthanarayanan, V., Schattat, M., Vogel, S. K., Krull, A., Pavin, N., & Tolić-Nørrelykke, I. M. (2013). Dynein Motion Switches from Diffusive to Directed upon Cortical Anchoring. *Cell*, *153*(7), 1526-1536. https://doi.org/10.1016/j.cell.2013.05.020

Boisvieux-Ulrich, E., Laine, M.-C., & Sandoz, D. (1987). In vitro effects of benzodiazepines on ciliogenesis in the quail oviduct. *Cell Motility and the Cytoskeleton*, *8*(4), 333-344. https://doi.org/10.1002/cm.970080406

Boisvieux-Ulrich, E., Lainé, M.-C., & Sandoz, D. (1989). In vitro effects of colchicine and nocodazole on ciliogenesis in quail oviduct. *Biology of the Cell*, *67*(1), 67-79. https://doi.org/10.1111/j.1768-322X.1989.tb03011.x

Boisvieux-Ulrich, E., Laine, M.-C., & Sandoz, D. (1989). *In vitro* effects of taxol on ciliogenesis in quail oviduct. *Journal of Cell Science*, *92*(1), 9-20. https://doi.org/10.1242/jcs.92.1.9

Boisvieux-Ulrich, E., Lainé, M.-C., & Sandoz, D. (1990). Cytochalasin D inhibits basal body migration and ciliary elongation in quail oviduct epithelium. *Cell and Tissue Research*, *259*(3), 443-454. https://doi.org/10.1007/BF01740770

Boudjema, A.-R., Al Jord, A., Lemaître, A.-I., Faucourt, M., Delgehyr, N., Spassky, N., & Meunier, A. (2024). Live-Imaging Centriole Amplification in Mouse Brain Multiciliated Cells. In V.

Mennella (Éd.), *Cilia* (Vol. 2725, p. 167-180). Springer US. https://doi.org/10.1007/978-1-0716-3507-0_10

Ching, K., Wang, J. T., & Stearns, T. (2022). Long-range migration of centrioles to the apical surface of the olfactory epithelium. *eLife*, *11*, e74399. https://doi.org/10.7554/eLife.74399

Gambarotto, D., Zwettler, F. U., Le Guennec, M., Schmidt-Cernohorska, M., Fortun, D., Borgers, S., Heine, J., Schloetel, J.-G., Reuss, M., Unser, M., Boyden, E. S., Sauer, M., Hamel, V., & Guichard, P. (2019). Imaging cellular ultrastructures using expansion microscopy (U-ExM). *Nature Methods*, *16*(1), 71-74. https://doi.org/10.1038/s41592-018-0238-1

Guirao, B., Meunier, A., Mortaud, S., Aguilar, A., Corsi, J.-M., Strehl, L., Hirota, Y., Desoeuvre, A., Boutin, C., Han, Y.-G., Mirzadeh, Z., Cremer, H., Montcouquiol, M., Sawamoto, K., & Spassky, N. (2010). Coupling between hydrodynamic forces and planar cell polarity orients mammalian motile cilia. *Nature Cell Biology*, *12*(4), 341-350. https://doi.org/10.1038/ncb2040

Hall, E. A., Kumar, D., Prosser, S. L., Yeyati, P. L., Herranz-Pérez, V., García-Verdugo, J. M., Rose, L., McKie, L., Dodd, D. O., Tennant, P. A., Megaw, R., Murphy, L. C., Ferreira, M. F., Grimes, G., Williams, L., Quidwai, T., Pelletier, L., Reiter, J. F., & Mill, P. (2023). Centriolar satellites expedite mother centriole remodeling to promote ciliogenesis. *eLife*, *12*, e79299. https://doi.org/10.7554/eLife.79299

Herawati, E., Taniguchi, D., Kanoh, H., Tateishi, K., Ishihara, S., & Tsukita, S. (2016). Multiciliated cell basal bodies align in stereotypical patterns coordinated by the apical cytoskeleton. *Journal of Cell Biology*, *214*(5), 571-586. https://doi.org/10.1083/jcb.201601023

Hirota, Y., Meunier, A., Huang, S., Shimozawa, T., Yamada, O., Kida, Y. S., Inoue, M., Ito, T., Kato, H., Sakaguchi, M., Sunabori, T., Nakaya, M., Nonaka, S., Ogura, T., Higuchi, H., Okano, H., Spassky, N., & Sawamoto, K. (2010). Planar polarity of multiciliated ependymal cells involves the anterior migration of basal bodies regulated by non-muscle myosin II. *Development*, *137*(18), 3037-3046. https://doi.org/10.1242/dev.050120

Ito, D., Zitouni, S., Jana, S. C., Duarte, P., Surkont, J., Carvalho-Santos, Z., Pereira-Leal, J. B., Ferreira, M. G., & Bettencourt-Dias, M. (2019). Pericentrin-mediated SAS-6 recruitment promotes centriole assembly. *eLife*, *8*, e41418. https://doi.org/10.7554/eLife.41418

Joukov, V., & De Nicolo, A. (2018). Aurora-PLK1 cascades as key signaling modules in the regulation of mitosis. *Science Signaling*, *11*(543), eaar4195. https://doi.org/10.1126/scisignal.aar4195

Kalkan, B. M., Ozcan, S. C., Quintyne, N. J., Reed, S. L., & Acilan, C. (2022). Keep Calm and Carry on with Extra Centrosomes. *Cancers*, *14*(2), 442. https://doi.org/10.3390/cancers14020442

Kalnins, V. I., Chung, C. K., & Turnbull, C. (1972). Procentrioles in ciliating and ciliated cells of chick trachea. *Zeitschrift Für Zellforschung Und Mikroskopische Anatomie*, *135*(4), 461-471. https://doi.org/10.1007/BF00583430

Kim, S., Chien, Y.-H., Ryan, A., & Kintner, C. (2022). Emi2 enables centriole amplification during multiciliated cell differentiation. *Science Advances*, *8*(13), eabm7538. https://doi.org/10.1126/sciadv.abm7538

Kim, S., Ma, L., Shokhirev, M. N., Quigley, I., & Kintner, C. (2018). Multicilin and activated E2f4 induce multiciliated cell differentiation in primary fibroblasts. *Scientific Reports*, *8*(1), 12369. https://doi.org/10.1038/s41598-018-30791-1

Kubo, A., Sasaki, H., Yuba-Kubo, A., Tsukita, S., & Shiina, N. (1999). Centriolar Satellites. *The Journal of Cell Biology*, *147*(5), 969-980. https://doi.org/10.1083/jcb.147.5.969

Kunimoto, K., Yamazaki, Y., Nishida, T., Shinohara, K., Ishikawa, H., Hasegawa, T., Okanoue, T., Hamada, H., Noda, T., Tamura, A., Tsukita, S., & Tsukita, S. (2012). Coordinated Ciliary Beating Requires Odf2-Mediated Polarization of Basal Bodies via Basal Feet. *Cell*, *148*(1-2), 189-200. https://doi.org/10.1016/j.cell.2011.10.052

Lemullois, M., Boisvieux-Ulrich, E., Laine, M.-C., Chailley, B., & Sandoz, D. (1988). Development and functions of the cytoskeleton during ciliogenesis in metazoa. *Biology of the Cell*, *63*(2),

195-208. https://doi.org/10.1016/0248-4900(88)90058-5

Li, W., Yi, P., Zhu, Z., Zhang, X., Li, W., & Ou, G. (2017). Centriole translocation and degeneration during ciliogenesis in *Caenorhabditis elegans* neurons. *The EMBO Journal*, *36*(17), 2553-2566. https://doi.org/10.15252/embj.201796883

Liu, H., Li, H., Jiang, Z., Jin, S., Song, R., Yang, Y., Li, J., Huang, J., Zhang, X., Dong, X., Mori, M., Fritzler, M. J., He, L., Cardoso, W. V., & Lu, J. (2023). A local translation program regulates centriole amplification in the airway epithelium. *Scientific Reports*, *13*(1), 7090. https://doi.org/10.1038/s41598-023-34365-8

Liu, Z., Nguyen, Q. P. H., Nanjundappa, R., Delgehyr, N., Megherbi, A., Doherty, R., Thompson, J., Jackson, C., Albulescu, A., Heng, Y. M., Lucas, J. S., Dell, S. D., Meunier, A., Czymmek, K., Mahjoub, M. R., & Mennella, V. (2020). Super-Resolution Microscopy and FIB-SEM Imaging Reveal Parental Centriole-Derived, Hybrid Cilium in Mammalian Multiciliated Cells. *Developmental Cell*, *55*(2), 224-236.e6. https://doi.org/10.1016/j.devcel.2020.09.016

LoMastro, G. M., Drown, C. G., Maryniak, A. L., Jewett, C. E., Strong, M. A., & Holland, A. J. (2022). PLK4 drives centriole amplification and apical surface area expansion in multiciliated cells. *eLife*, *11*, e80643. https://doi.org/10.7554/eLife.80643

Marthiens, V., Piel, M., & Basto, R. (2012). Never tear us apart – the importance of centrosome clustering. *Journal of Cell Science*, *125*(14), 3281-3292. https://doi.org/10.1242/jcs.094797

Megraw, T. L., Kilaru, S., Turner, F. R., & Kaufman, T. C. (2002). The centrosome is a dynamic structure that ejects PCM flares. *Journal of Cell Science*, *115*(23), 4707-4718. https://doi.org/10.1242/jcs.00134

Mercey, O., Al Jord, A., Rostaing, P., Mahuzier, A., Fortoul, A., Boudjema, A.-R., Faucourt, M., Spassky, N., & Meunier, A. (2019). Dynamics of centriole amplification in centrosome-depleted brain multiciliated progenitors. *Scientific Reports*, *9*(1), 13060. https://doi.org/10.1038/s41598-019-49416-2

Mercey, O., Levine, M. S., LoMastro, G. M., Rostaing, P., Brotslaw, E., Gomez, V., Kumar, A.,

Spassky, N., Mitchell, B. J., Meunier, A., & Holland, A. J. (2019). Massive centriole production can occur in the absence of deuterosomes in multiciliated cells. *Nature Cell Biology*, *21*(12), 1544-1552. https://doi.org/10.1038/s41556-019-0427-x

Mori, M., Hazan, R., Danielian, P. S., Mahoney, J. E., Li, H., Lu, J., Miller, E. S., Zhu, X., Lees, J. A., & Cardoso, W. V. (2017). Cytoplasmic E2f4 forms organizing centres for initiation of centriole amplification during multiciliogenesis. *Nature Communications*, *8*(1), 15857. https://doi.org/10.1038/ncomms15857

Nabais, C., Pessoa, D., de-Carvalho, J., Van Zanten, T., Duarte, P., Mayor, S., Carneiro, J., Telley, I. A., & Bettencourt-Dias, M. (2021). Plk4 triggers autonomous de novo centriole biogenesis and maturation. *Journal of Cell Biology*, *220*(5), e202008090. https://doi.org/10.1083/jcb.202008090

Nanjundappa, R., Kong, D., Shim, K., Stearns, T., Brody, S. L., Loncarek, J., & Mahjoub, M. R. (2019). Regulation of cilia abundance in multiciliated cells. *eLife*, *8*, e44039. https://doi.org/10.7554/eLife.44039

Nigg, E. A., & Holland, A. J. (2018). Once and only once: Mechanisms of centriole duplication and their deregulation in disease. *Nat Rev Mol Cell Biol*, *19*(5), 297-312. https://doi.org/10.1038/nrm.2017.127

Odabasi, E., Gul, S., Kavakli, I. H., & Firat-Karalar, E. N. (2019). Centriolar satellites are required for efficient ciliogenesis and ciliary content regulation. *EMBO Reports*, *20*(6), e47723. https://doi.org/10.15252/embr.201947723

Pitaval, A., Senger, F., Letort, G., Gidrol, X., Guyon, L., Sillibourne, J., & Théry, M. (2017). Microtubule stabilization drives 3D centrosome migration to initiate primary ciliogenesis. *Journal of Cell Biology*, *216*(11), 3713-3728. https://doi.org/10.1083/jcb.201610039

Revinski, D. R., Zaragosi, L.-E., Boutin, C., Ruiz-Garcia, S., Deprez, M., Thomé, V., Rosnet, O., Gay, A.-S., Mercey, O., Paquet, A., Pons, N., Ponzio, G., Marcet, B., Kodjabachian, L., & Barbry, P. (2018). CDC20B is required for deuterosome-mediated centriole production in

multiciliated cells. *Nature Communications*, *9*(1), 4668. https://doi.org/10.1038/s41467-018-06768-z

Ruiz García, S., Deprez, M., Lebrigand, K., Cavard, A., Paquet, A., Arguel, M.-J., Magnone, V., Truchi, M., Caballero, I., Leroy, S., Marquette, C.-H., Marcet, B., Barbry, P., & Zaragosi, L.-E. (2019). Novel dynamics of human mucociliary differentiation revealed by single-cell RNA sequencing of nasal epithelial cultures. *Development*, *146*(20), dev177428. https://doi.org/10.1242/dev.177428

Sedzinski, J., Hannezo, E., Tu, F., Biro, M., & Wallingford, J. B. (2017). RhoA regulates actin network dynamics during apical surface emergence in multiciliated epithelial cells. *Journal of Cell Science*, *130*(2), 420-428. https://doi.org/10.1242/jcs.194704

Sorokin, S. P. (1968). Reconstructions of centriole formation and ciliogenesis in mammalian lungs. *Journal of Cell Science*, *3*(2), 207-230. https://doi.org/10.1242/jcs.3.2.207

Strnad, P., Leidel, S., Vinogradova, T., Euteneuer, U., Khodjakov, A., & Gönczy, P. (2007). Regulated HsSAS-6 Levels Ensure Formation of a Single Procentriole per Centriole during the Centrosome Duplication Cycle. *Developmental Cell*, *13*(2), 203-213. https://doi.org/10.1016/j.devcel.2007.07.004

Tateishi, K., Nishida, T., Inoue, K., & Tsukita, S. (2017). Three-dimensional Organization of Layered Apical Cytoskeletal Networks Associated with Mouse Airway Tissue Development. *Scientific Reports*, *7*(1), 43783. https://doi.org/10.1038/srep43783

Tozer, S., Baek, C., Fischer, E., Goiame, R., & Morin, X. (2017). Differential Routing of Mindbomb1 via Centriolar Satellites Regulates Asymmetric Divisions of Neural Progenitors. *Neuron*, *93*(3), 542-551.e4. https://doi.org/10.1016/j.neuron.2016.12.042

Vale, R. (1985). Movement of organelles along filaments dissociated from the axoplasm of the squid giant axon. *Cell*, *40*(2), 449-454. https://doi.org/10.1016/0092-8674(85)90159-X

Vladar, E. K., & Stearns, T. (2007). Molecular characterization of centriole assembly in ciliated epithelial cells. *The Journal of Cell Biology*, *178*(1), 31-42.

https://doi.org/10.1083/jcb.200703064

Vladar, E. K., Stratton, M. B., Saal, M. L., Salazar-De Simone, G., Wang, X., Wolgemuth, D., Stearns, T., & Axelrod, J. D. (2018). Cyclin-dependent kinase control of motile ciliogenesis. *eLife*, *7*, e36375. https://doi.org/10.7554/eLife.36375

Yamamoto, S., & Kitagawa, D. (2019). Self-organization of Plk4 regulates symmetry breaking in centriole duplication. *Nature Communications*, *10*(1), 1810. https://doi.org/10.1038/s41467-019-09847-x

Zhao, H., Chen, Q., Fang, C., Huang, Q., Zhou, J., Yan, X., & Zhu, X. (2019). Parental centrioles are dispensable for deuterosome formation and function during basal body amplification. *EMBO Reports*, *20*(4), e46735. https://doi.org/10.15252/embr.201846735

Zhao, H., Chen, Q., Li, F., Cui, L., Xie, L., Huang, Q., Liang, X., Zhou, J., Yan, X., & Zhu, X. (2021). Fibrogranular materials function as organizers to ensure the fidelity of multiciliary assembly. *Nature Communications*, *12*(1), 1273. https://doi.org/10.1038/s41467-021-21506-8

Zhao, H., Zhu, L., Zhu, Y., Cao, J., Li, S., Huang, Q., Xu, T., Huang, X., Yan, X., & Zhu, X. (2013). The Cep63 paralogue Deup1 enables massive de novo centriole biogenesis for vertebrate multiciliogenesis. *Nature Cell Biology*, *15*(12), 1434-1444. https://doi.org/10.1038/ncb2880

## Acknowledgements

We thank all the members of the Spassky lab who contributed in the elaboration of this research work, Chris Kintner for sharing the adenoviral vectors for the expression of MCIDAS-E2F4-Dp1 and Xavier Morin for sharing the MEFs cells. We are thankful to the IBENS administrative team and imaging platform for their support, and to the IBENS Animal Facility for animal care. The team was funded by the Agence Nationale de la Recherche Investissements d'Avenir (ANR-10-LABX-54 MEMO_LIFE and ANR-11-IDEX-0001-02_PSL* Research University). The Spassky team is supported by Inserm, the CNRS, the École Normale Supérieure (ENS), the ANR (ANR-20-CE45-0019, ANR-21-CE16-0016, and ANR-22-CE16-0011), the Fondation pour la Recherche Médicale (FRM EQU202103012767), and the European Research Council (ERC Consolidator grant 647466). A-R.B received a fellowship from La ligue and the Labex MEMOLIFE.

## Author contributions

A-R. B, R. B. designed, performed and analyzed the majority of the experiments, with C. E. J performing all the U-ExM and FRAP experiments, O. M. providing the first data on the role of microtubules in centriole amplification, A. A. J. having performed some of the movies analyzed in this study and M. F. providing general cell culture support. G. L. M., C. E. J. and A. J. H. designed, produced and validated the Plk4 antibody and the mRuby-Deup1 mice. All the experiments of MEFs on micropatterns were performed in the lab of M.T with the support of A. S. A-R. B., R. B. C. E. J, N. D., N. S., A.J. H. and A.M. analyzed the data. A. M. conceived and supervised the study. A-R. B., R. B, C. E. J., A. M. co-wrote the manuscript.

**Competing interests**: Authors declare that they have no competing interests.

# Figure captions

**Figure 1: MEF-MCCs grown on micropatterns highlight the pericentrosomal focalization of procentriole production**

**(A)** Scheme of the MEF-MCC differentiation process on crossbow micropatterns.

**(B)** MCC-induced fibroblasts on micropatterns perform the typical step-wise dynamics of centriole amplification. Representative immunofluorescence images of MEF-MCC on crossbow micropatterns showing the 4 stages of differentiation. Scale bar, 10 µm.

**(C)** Density mapping of centrosome in MEF-MCCs before amplification (centrosome stage, left column), and procentrioles during early amplification (cells with less than 10 SAS6 focis/cell, middle column) or late amplification (cells with more than 10 SAS6 focis/cell, right column) treated with DMSO (top row) and Nocodazole 1µM (bottom row). Three independent experiments were quantified. Scale bar, 10 µm.

**(D)** Density mapping of PCNT fluorescence signal during centrosome stage (left column) early A-stage (middle column) and late A-stage (right column) in MEF-MCCs under DMSO (top row) and Nocodazole 1µM (bottom row). Insets on the right of each panel is a representative cell used for the density mapping. Two independent experiments were quantified. Scale bar, 10 µm.

DM1A marks all MT, YL1/2 marks tyrosinated MT, SAS6 marks procentrioles, GT335 marks centrosome, mature procentrioles and cilia, PCNT marks pericentrin. Dotted lines show the crossbow shape of the micropattern, white graduated lines show x and y axes. Insets on the right of each panel is a representative cell used for the density mapping.

**Figure 2: Deup1 is a centrosomal protein and assembles deuterosomes in the pericentrosomal region in brain MCC**

**(A)** Scheme of the ependymal cell culture protocol. Eye shows which stage is observed.

**(B)** Cen2-GFP; mRuby-Deup1 dynamics of the new mouse line during centriole amplification. The previously described stages of centriole amplification can be identified with the Cen2-GFP signal. The procentrioles are seen organizing around the endogenous mRuby3-Deup1+ deuterosomes in A-, G- and D-stage. Scale bar, 5µm.

**(C)** Early A-stage dynamics in Cen2-GFP; mRuby-Deup1+ cells. The horizontal blue bar illustrates the newly observed “cloud” stage where a Deup1+ cloud forms, before the A-

phase (05:00), around the parental centrioles. The horizontal grey bar illustrates the previously described "Amplification" A-stage, where Cen2-GFP+/mRuby3-Deup1+ procentriole loaded deuterosomes exit the cloud (7:00 – 12:00, arrows). White dotted circles enclose parental centrioles. The white and black cross rules out the Cen2-GFP+ aggregate not to be mistaken with a centrosome; dt=1h; Cen2-GFP in green, Deup1 in red; scale bar, 5 µm. See Video 1.

**(D)** Cen2-GFP and mRuby-Deup1 dynamics during the cloud stage. Cen2-GFP+ and mRuby-Deup1+ foci are not always colocalized. Yellow dotted circles enclose parental centrioles. Deup1+ foci can interact persistently with one parental centriole. dt=1h; Cen2-GFP in green, Deup1 in red. Scale bar, 5µm. See Video 2.

**(E)** mRuby-Deup1+ signal during the cloud stage in Cen2-GFP cells. Deup1 foci are color-coded with arrowheads to appreciate their oscillatory behaviors towards the centrosomal mRuby-Deup1+cloud; green shades enclose parental centrioles that were localized using Cen2-GFP signal that is not visible here. See associated video. dt=5s; scale bar, 5µm. See Video 3.

**(F)** mRuby-Deup1+ intermittent interaction with one parental centriole in Cen2-GFP+ cells. Deup1+ foci indicated by white arrow head oscillates to and from one parental centriole in yellow dotted circles. dt=5s; scale bar, 5 µm. See Video 4.

**(G)** Early deuterosome oscillating behavior during A-stage. White arrows show deuterosomes back and forth movements towards the centrosomal cloud; blue arrows show a deuterosome moving to the cytoplasm and away from other deuterosomes. dt=5s; scale bar, 5 µm. See Video 5.

**Figure 3: Procentriole assembly begins in a pericentrosomal nest and continues during radial migration**

**(A-C)** Representative U-ExM images of brain MCCs during cloud stage. Cells were immunostained with antibodies to β-tubulin, Centrin, Deup1 (A), β-tubulin, SAS6, Deup1 (B), or β-tubulin, PLK4, Cen (C). mc: mother centriole, dc: daughter centriole.

**(D-F)** Representative U-ExM images of brain MCCs during early A-stage. Cells were immunostained with antibodies to β-tubulin, Centrin, Deup1 (D), β-tubulin, SAS6, Deup1

(E), or Acetylated-tubulin, PLK4, Deup1 (F). Arrows mark Deup1 foci with either centrin (D) or procentrioles (E, F). mc: mother centriole, dc: daughter centriole.

**(G-I)** Representative U-ExM images of brain MCCs during late A-stage. Boxes denote zoomed in regions on right, with 1-4 labels marking increasing distance from the parent centrioles. Cells were immunostained with antibodies to β-tubulin, SAS6, Deup1 (G), Acetylated-tubulin, PLK4, Deup1 (H), or β-tubulin, Centrin, Acetylated-tubulin (I). mc: mother centriole, dc: daughter centriole.

**(J)** Quantitation showing the procentriole distance from parents is shorter in procentrioles without αβ-tubulin compared to procentrioles with αβ-tubulin. SAS6 is used as a marker for procentrioles associated with deuterosomes. Graphs show mean ± SD from n=7 cells across 3 different experiments. ****p<0,0001 using unpaired t-test.

**(K)** Quantitation showing the procentriole distance from parents is shorter in procentrioles without Acetylated-tubulin compared to procentrioles with Acetylated-tubulin. PLK4 is used as a marker for procentrioles associated with deuterosomes. Graphs show mean ±SD from n=3 cells across 3 different experiments. ****p<0,0001 using unpaired t-test.

**(L)** Quantitation showing procentriole length measured by β-tubulin increases with distance from parents during A-stage. Graphs show mean ±SD from n=10 cells across 3 different experiments.

**(M)** Quantitation showing procentriole width measured by β-tubulin increases with distance from parents during A-stage. Graphs show mean ±SD from n=10 cells across 3 different experiments.

**(N)** Quantitation comparing percent of cells showing Deup1 enrichment at daughter centriole over mother centriole (DC>MC), equal enrichment at both parent centrioles (DC = MC), or enrichment at mother centriole over daughter centriole (MC>DC) in cloud-stage and A-stage. A total of 54 cells were analyzed across 3 experiments.

**(O)** Table summarizing protein localization as visualized by U-ExM during cloud, early A-, and late A-stage. “+” indicates protein is present; “–” indicates not present.

**(P)** Scheme representing cloud and A-phase progression in time and space.

**Figure 4: Microtubules organize the pericentrosomal nest, promote deuterosome growth and hinder the dispersion of deuterosomes**

**(A)** Immunostaining profiles of procentrioles and microtubules during brain Cen2-GFP MCC differentiation. Procentrioles were counter-stained with anti-SAS6 antibodies (red), dynamic tyrosinated MTs were counter-stained with YL1-2 antibodies and the nucleus was counter-stained with Hoechst (blue). All micrographs are max projections of whole z-stacks except for the MCC-stage where max were done from apical or basal z-stacks selected from the same cell. White and red arrow heads show parental centrioles. Scale bar, 5 µm.

**(B)** Cen2-GFP; mRuby-Deup1 profiles in control and Nocodazole (10µM) treated A-stage cell. t0 corresponds to the first acquisition when cells were still untreated. White arrows indicate the centrosomal centrioles. **Top row:** at t+3h and 10h after DMSO addition, the procentriole-loaded deuterosomes stay in a restricted area around the pericentrosomal region. Plain white line outlines the border of the cell; plain blue lines enclose the area of the Cen2-GFP; mRuby-Deup1+ deuterosomes in control cells; blue dotted lines enclose the area of the Cen2-GFP; mRuby-Deup1+ cloud. **Bottom row:** At t+3h after Nocodazole (10µM) addition, the procentriole-loaded deuterosomes disperse and appear scattered in the cell, covering almost the whole cell surface at t+10h. Plain white line outlines the border of the cell; plain orange line encloses the area of Cen2-GFP; mRuby-Deup1+ deuterosomes; orange dot line encloses the area of the Cen2-GFP; mRuby-Deup1+ cloud; the black cross rules out the Cen2-GFP+ aggregate not to be mistaken with a centrosome. dt=40min; scale bar, 5µm. See Video 6.

**(C)** Quantification of the area occupied by the mRuby-Deup1 signal over time in cloud stage in control (DMSO) and Nocodazole (10µM) treated cells represented by the dotted blue and orange lines respectively in (B). Black arrow indicates that Nocodazole and DMSO were added right after the first acquisition. Three independent experiments were analyzed, n=12 DMSO cells, n=14 Noco 10µM cells. dt=40min; ****p<0,0001; non-parametric Mann Whitney test; error bars represent mean ± SD.

**(D)** Quantification of the area occupied by the deuterosomes over time in A-stage cells under DMSO and acute Nocodazole 10µM treated cells represented by the plain blue and orange lines respectively in (B). Black arrow indicates that Nocodazole and DMSO were added right after the first acquisition. Three independent experiments were analyzed, n=12 DMSO cells; n= 15 Noco 10µM cells. dt=40min; ****p<0,0001; non-parametric Mann Whitney test; error bars represent mean ± SD.

**(E**) Super resolution immunostaining profile of deuterosomes (Deup1) and procentrioles (SAS6) under Nocodazole (10µM, 24h). Deuterosomes are reduced to small subunits scarcely loaded with procentrioles. Scale bar, 5 µm.

**(F)** Quantification of the percentage of "cloud" and A-stage cells displaying at least one Deup1 foci oscillation to and from the centrosome during 1-4min movies at dt5-15s, in DMSO and acute Nocodazole (10µM) treated cells. Three independent experiments were scored, n=25 DMSO cells, n=20 Noco 10µM cells analyzed. ****p=0.0001; Chi-square test.

**(G)** Quantification of deuterosome size in A and G-stage cells (pooled) under DMSO and Nocodazole chronic treatments (48h; 1µM and 5µM). Three independent experiments were scored, n=80 DMSO cells, n=43 Noco 1µM cells, n=63 Noco 5µM cells. Error bars represent mean ± SD. **** P<0.0001; ***p=0.0002; **p=0.0025; non-parametric Mann Whitney test.

**(H)** Quantification of centriole number per deuterosome in G-stage cells under DMSO and Nocodazole chronic treatments (48h; 1µM and 5µM). Three independent experiments were scored, n=11 DMSO cells, n=17 Noco 1µM cells, n=21 Noco 5µM cells. Error bars represent min to max ± median. **** P<0.0001; non-parametric Mann Whitney test.

**(I)** Quantification of the deuterosome number per cell in A and G-stage cells (pooled) under DMSO and Nocodazole chronic treatments (48h; 1µM and 5µM). Three independent experiments were scored, n=80 DMSO cells, n=43 Noco 1µM cells, n=63 Noco 5µM cells. Error bars represent min to max ± median. **** P<0.0001; ***p=0.0002; **p=0.0025; non-parametric Mann Whitney test.

**(J)** Quantification of SAS6+ centriole number in G- and D-stage (pooled) brain cells under DMSO and Nocodazole chronic treatments (48h; 1µM and 5µM). Three independent experiments were scored; error bars represent min to max ± median. n=42 DMSO cells, n=34 Noco 1µM; n= 29 Noco 5µM cells analyzed. Error bars represent min to max ± median. ns, not significant; ** p=0,002; non-parametric Mann Whitney test.

**Figure 5: Amplified procentrioles convert to multiple microtubule organizing centers (MTOC) during the amplification (A) to growth (G) transition**

**(A-B)** Representative immuno-reactivity profile of PCNT and Plk1 in A- and G-phases in Cen2-GFP+ brain MCC progenitors. Dotted line square surrounds procentrioles shown in the magnified view. Scale bar, 5µm.

**(C-D)** Quantification of PCNT and Plk1 intensities on procentrioles in A- and G-stage brain MCCs. Fluorescence intensity was normalized on PCNT and Plk1 intensity of the centrosome of one non-differentiating neighboring cell. Three independent experiments were scored for both stainings; n= 19 PCNT cells, n= 32 PLK1 cells analyzed; error bars represent mean ± SD. ****p<0,0001; non-parametric Mann Whitney test.

**(E-G)** Immunostaining profile of YL1/2 in Cen2-GFP+ brain MCCs (E) and Sas6 stained MEF-MCCs (G) in A- and G-stage after repolymerization experiment. Dot lined square surrounds a procentriole shown in the magnified view. White arrowheads indicate centrosomal centrioles. Three independent experiments were scored for each brain or MEF-MCCs. Scale bar, 10 µm.

**(F-H)** Quantification of YL1/2 intensity in A-stage and G-stage brain MCCs (F) and MEF-MCCs (H). Fluorescence intensity was normalized on the centrosome of one non-differentiating neighboring cell. Three independent experiments were quantified for brain MCCs (F) n= 56 cells. Three independent experiments were quantified for MEF-MCCs (H) n= 46 cells. Error bars represent mean ± SD; ****p<0,0001; non-parametric Mann Whitney test.

**Figure 6: Microtubules are required for procentriole attachment to the nuclear membrane and efficient disengagement**

**(A)** Cen2-GFP+ dynamics from G-stage to migration stage. **Top line:** time-lapse images showing perinuclear distribution of centrioles at G-stage (00:00); perinuclear disengagement of centrioles from deuterosomes (empty flowers) and parental centrioles (plain flowers, arrows) in a Cen2-GFP+ cell (4:30); release of centrioles from the nuclear membrane (6:30) for apical migration (from 10:00). **Bottom line:** profile view of the Cen2-GFP+ signal dynamics. Dotted white line outlines the nucleus identified by contrasting Cen2-GFP signal. dt=30min, scale bar, 5 µm. See Videos 7.

**(B)** Magnified view of a Cen2-GFP; mRuby-Deup1 flower dynamics in G-stage. White arrowheads indicate the procentriole-loaded deuterosomes migrating on the nuclear envelope; dotted white line outlines the nucleus identified by contrasting Cen2-GFP signal. dt=5s, scale bar, 2 µm. See Video 9.

**(C)** Quantification of the duration of the interaction between procentriole-loaded deuterosome and the nuclear envelope before D-stage in Cen2-GFP brain MCCs. Four independent experiments quantified, n=75 flower, n=8 cells analyzed. Error bars represent min to max ± median.

**(D)** Schematic representation of brain MCC differentiation depicting the timing of MT depolymerisation treatment. The eye shows the amplification stage monitored.

**(E)** Immuno-reactivity of Deup1 on Cen2-GFP brain MCCs during G-stage, treated acutely with DMSO or Nocodazole (10µM, 4h). The nucleus is counter-stained with Hoechst. Scale bar, 5µm.

**(F)** Quantification of the percentage of tethered deuterosomes per G-stage cell in DMSO and Nocodazole (10µM, 4h). Four independent experiments quantified; n=75 deuterosomes in DMSO, n=31 deuterosomes in Nocodazole. Error bars represent mean ± SD; ****p<0,0001; Chi-2 test with Yates' correction.

**(G)** Quantification of the proportion of procentrioles disengaging with a nuclear contact. Three independent experiments were quantified; n=98 flowers, n=8cells.

**(H)** Schematic representation of brain MCC differentiation depicting the timing of MT depolymerisation treatments. The eye shows the amplification stage monitored.

**(I)** Quantification of the proportion of D-stage cells per fields among amplifying cells under chronic DMSO and Nocodazole treatments (48h, 1µM and 5µM). At least three independent experiments were quantified, n=2626 DMSO cells, n=1483 Noco 1µM cells, n=909 Noco 5µM cells; error bars represent mean ± SD. ns, not significant; ****p<0,0001; non-parametric Mann Whitney test.

**(J)** Quantification of D-stage quality phenotype under chronic DMSO and Nocodazole (48h, 1µM). Total disengagement in black, partial disengagement in white. At least three independent experiments were quantified, n=35 DMSO cells analyzed, n=25 Noco 1µM cells analyzed. ****p<0,0001; Chi-2 test with Yates' correction.

**(K)** Quantification of disengagement duration in Cen2-GFP brain MCCs under DMSO and acute Nocodazole treatment (10µM). Three independent experiments were quantified, n=16

DMSO cells analyzed, n=11 Noco 10µM cells analyzed. *p=0,0235; non-parametric Mann Whitney test.

**(L)** Representative movie of Cen2-GFP dynamics in D-stage of brain MCCs under DMSO and acute Nocodazole treatment (10µM). (t-1) represents the timepoint before drug treatments. At t+3h45, the DMSO cell centrioles are almost all disengaged while in Nocodazole 10µM, some flowers are not disengaged yet. At t+11h20, the control cell displays a regrouped patch of centrioles whereas Nocodazole cell shows some scattered centrioles that cover the whole surface of the cytoplasm. dt=5min; scale bar, 5 µm. See Video 12.

**Figure 7: Disengagement of centrioles is a combination of centriole individualization and deuterosome splitting or dissolution**

**(A)** Cen2-GFP; mRuby-Deup1 dynamics in D-stage. Upper panels: in early D-stage (00:00), some procentrioles are already individualized, separated from Deup1+ deuterosomes as shown by the white arrows. During D-stage, procentrioles disengaged from deuterosomes can keep a subunit of Deup1 in their proximal portion (red arrows, 1:40), splitting them in smaller entities bearing fewer procentrioles not disengaged yet (4:10), as well as Deup1 signal dissolution. Lower panels: grayscale showing the initial pool of 19 deuterosomes (00 :00) splitting to 32 Deup1+ foci (4 :10). dt=50min; scale bar, 5 µm. See Video 13.

**(B-C)** Quantification of the size and number of deuterosomes per cell over time in D-stage relative to G-stage. n=10 cells analyzed were plotted individually to reveal the tendency to decrease in size, while increasing the number of Deup1 foci. Each measurement in D-stage was normalized on G-stage. Three independent experiments were scored; error bars represent mean ± SD.

**(D)** Splitted deuterosomes with a single centriole migrating away from each other on the nuclear envelope. White dotted line outlines shadow of the nuclear membrane identified with contrasting Cen2-GFP signal. dt=5s, scale bar, 2 µm. See Video 14.

**(E)** Tyrosinated microtubules and deuterosomes immuno-reactivity profiles in brain MCC in D-stage. These pictures show one z plane in the basal part of the cell. Tyrosinated MTs were stained with (YL 1-2) and deuterosomes with Deup1. Deup1 signal intensity is decreased

from left to right to show that deuterosomes are located on MT nodes. Scale bar, 5 µm. See Video 16.

**(F)** Representative U-ExM image of brain MCCs during G-stage. Cells were immunostained with antibodies to Acetylated-tubulin, Deup1, and the nucleus was counter stained with Hoechst. Scale bar, 1µm. Right insets show magnification of a deuterosome bearing multiple procentrioles. Scale bar, 250nm.

**(G)** Representative U-ExM images of brain MCCs during D-stage. Cells were immunostained with antibodies to Acetylated-tubulin, Deup1, and the nucleus was counter stained with Hoechst. Scale bar, 1µm. Right insets show: (top) single centrioles disengaged from deuterosomes and empty deuterosomes; (bottom) small deuterosomes with single centrioles. Scale bar, 250nm.

**Figure 8: Disengaged centrioles finally converge with the former centrosome in a microtubule-dependent manner**

**(A)** Quantification of the relative frequency of the centriole position regarding the centrosomal centriole (CC) at the end of centriole individualization (green) and the end of apical migration (red). Bottom: representative apical projections of segmented Cen2-GFP+ centrioles at the end of centriole individualization (green frame) and the end of apical migration (red frame). Green arrow shows the centrosome which served as the reference point; the nucleus is in dark blue. n=3 cells; scale bar, 5 µm.

**(B)** Manual single centriole 3D tracking reveals convergence of centrioles towards the centrosome region. Top left panel: apical view of manually tracked migrating centrioles trajectories. Top right panel: apical view of the directionality vectors of the migrating centrioles. Bottom panel: corresponding profile views of the top panels. dt=5min; scale bar, 5 µm. See Video 17.

**(C)** Evolution of individual centriole distance to centrosome over time. dt=5min. Three independent experiments were analyzed, n=33 centriole trajectories in n=5 cells.

**(D)** Example of the single blue centriole trajectory from (B) towards the centrosome in the XY plane and in the Z plane. Yellow dots represent the steps of apical migration. The origin represents the position of the centrosome.

**(E)** Evolution of the Z coordinates during the apical migration of 16 centrioles from 5 cells. Three independent experiments were analyzed. The origin represents the Z position of the centrosome. dt=5min.

**(F)** Speed of migration plotted from all 953 steps of 33 migrating centrioles versus the 74 extracted steps of apical migration of the 16 centrioles basally located in the cells. Box and whiskers plots (2,5-97,5 percentile). See distribution in Fig. 8 Supplementary 1C.

**(G)** Schematic representation of brain MCC differentiation depicting the timing of MT depolymerisation treatment. The eye shows the amplification stage monitored.

**(H)** Profile view of centriole apical migration after D-stage in Cen2-GFP+ DIV2 brain MCCs treated with acute DMSO and Nocodazole 10µM. At t-1, cells display late G-stage/early D-stage procentrioles and are not treated with any drug. DMSO and Nocodazole 10µm were added right after the first timepoint acquisition. In DMSO, 2 centriole patches are under and over the nucleus (t+0h). The patch under the nucleus progressively joins the apical one (t+2h) to become one apical patch (t+4h) and stabilizes (t+6h). In 10µM Nocodazole, procentrioles start to scatter after 1h, and the group of centrioles below the nucleus travel up and down (t+2h and t+4h) and does not succeed to become one apical group of centrioles (t+6h). Four independent experiments were scored for n=7 DMSO cells and two independent experiment were scored for n=4 Noco 10µM cells. dt=5min; scale bar, 5 µm. See Video 18.

**(I)** Quantification of apical migration duration in DMSO and acute Nocodazole 10µM in brain MCCs. Four independent experiments were scored for n=7 DMSO cells and two independent experiment were scored for n=4 Noco 10µM cells. Error bars represent min to max ± median. ****p<0,0001; non-parametric Mann Whitney test.

**(J)** Quantification of MBB patch area (µm²) in DMSO and chronic Nocodazole treatment (48h, 1 and 5µM) in brain MCCs. Three independent experiments were scored, n=22 DMSO cells analyzed, n=15 Noco 1µM cells and n=18 Noco 5µM cells. Error bars represent min to max ± median. ****p<0,0001; non-parametric Mann Whitney test.

**Figure 9**

**Model proposed by this study on the role of microtubules in centriole amplification in brain MCC.**

**Progenitor stage:** Undifferentiated brain MCC progenitor. The centrosome is close to the apical membrane, the mother centriole is docked and templates the primary cilium. At this stage, MTs are organized by the centrosome.

**Amplification stage:** MTs organize a Deup1, Centrin and PCNT nest around the centrosome from which new centrioles emerge. In the earliest step of amplification, a Centrin, Deup1 and PCNT cloud (pink area) appears around the centrosomal centrioles, in a MT dependent fashion. Then, early Plk4+, SAS6+, Cen2-GFP+ procentrioles form on small Deup1+ structures emerge. Procentrioles don't have a MT wall yet (small blue procentrioles). Once they accumulate, they start exiting the cloud, and are maintained by the MTs in a restricted area around this pericentrosomal nest. As procentriole loaded deuterosomes migrate away from the cloud, a growing number of procentrioles recruit tubulin, building MT centriolar walls. These microtubules are progressively acetylating (pink centriole walls).

**Growth stage: Procentrioles become MT nucleators and MTs anchor procentrioles to the nuclear membrane.** In this stage, procentrioles mature on deuterosomes and parental centrioles by acquisition of polyglutamylated tubulin (blue centriole walls). Concomitantly, they migrate towards the nuclear membrane through a MT dependent mechanism where they distribute almost isotropically. They stay associated to the nuclear membrane along which they are able to migrate thanks to MT related mechanisms.

**Disengagement stage: MTs contribute to the centrioles' disengagement.** Upon APC/C, Plk1 and MT actions, centrioles disengage from the deuterosomes and parental centrioles. Disengagement from deuterosomes consists of centriole detachment from deuterosomes, deuterosome splitting and Deup1 disintegration. Some Deup1 agregates (centriole free) can remain in the cytoplasm until ciliation.

**Migration stage: MTs help centrioles reach their docking site.** Once all centrioles are individualized, they start migrating collectively from the basal pole and periphery of the cell, with the help of MTs, towards the apical membrane where the former parental centrioles stand and dock.

# Graphical Abstract

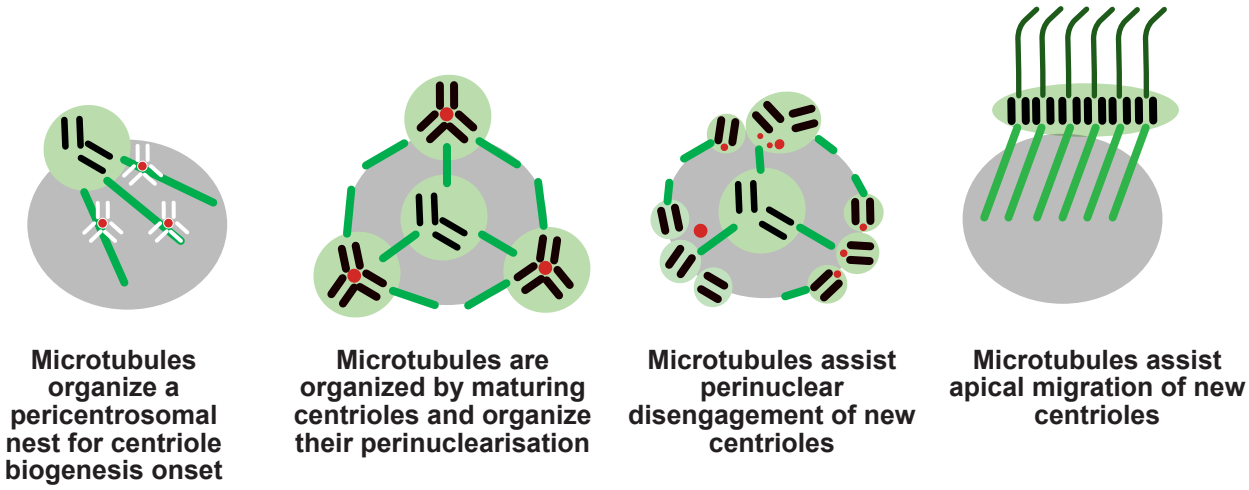

# Figure 1

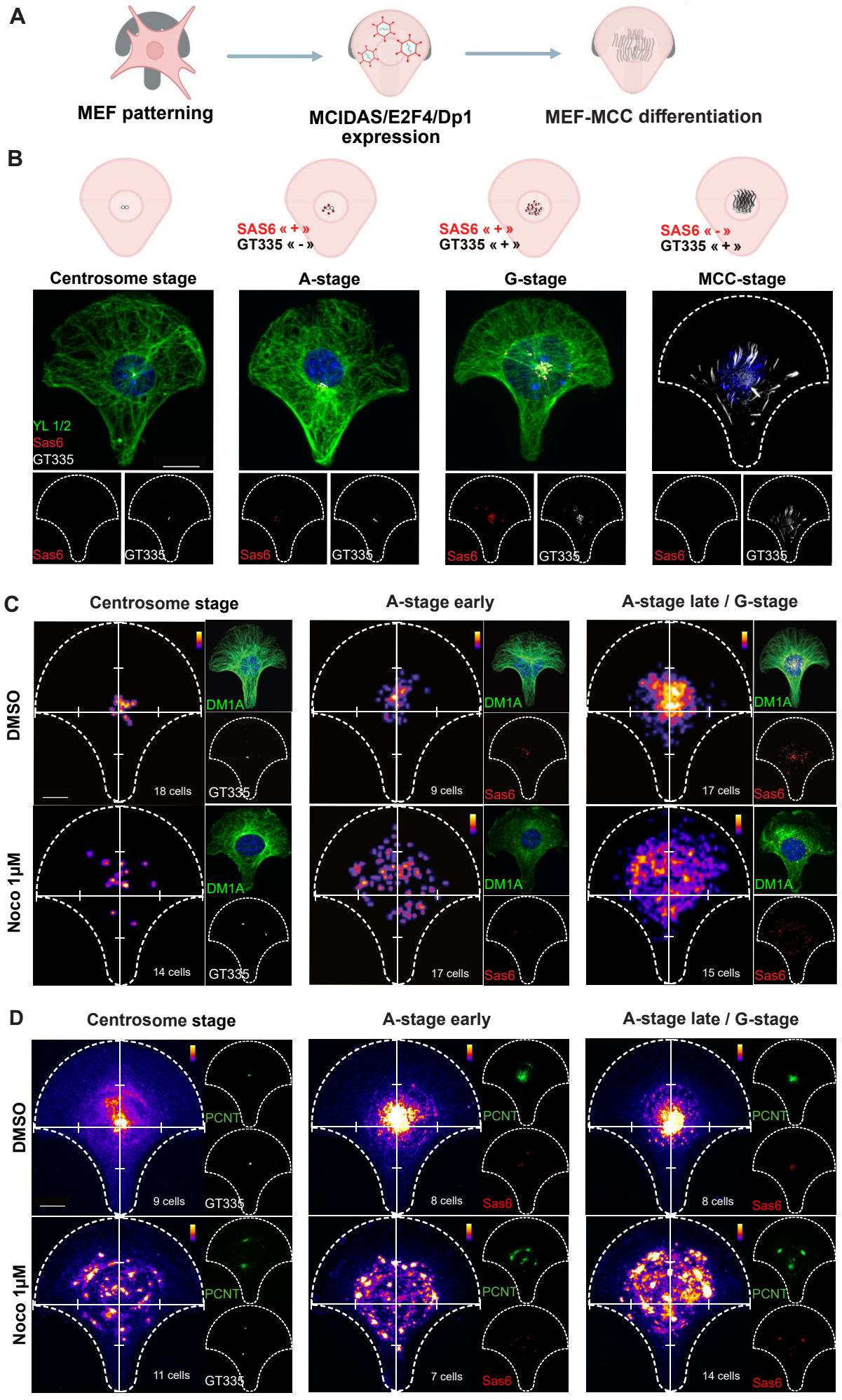
A
MEF patterning
MCIDAS/E2F4/Dp1 expression
MEF-MCC differentiation
B
SAS6 « + »
GT335 « - »
SAS6 « + »
GT335 « + »
SAS6 « - »
GT335 « + »
Centrosome stage
A-stage
G-stage
MCC-stage
YL 1/2
Sas6
GT335
C
Centrosome stage
A-stage early
A-stage late / G-stage
DMSO
Noco 1µM
DM1A
GT335
Sas6
18 cells
9 cells
17 cells
14 cells
17 cells
15 cells
D
Centrosome stage
A-stage early
A-stage late / G-stage
DMSO
Noco 1µM
PCNT
GT335
Sas6
9 cells
8 cells
8 cells
11 cells
7 cells
14 cells

# Figure 2

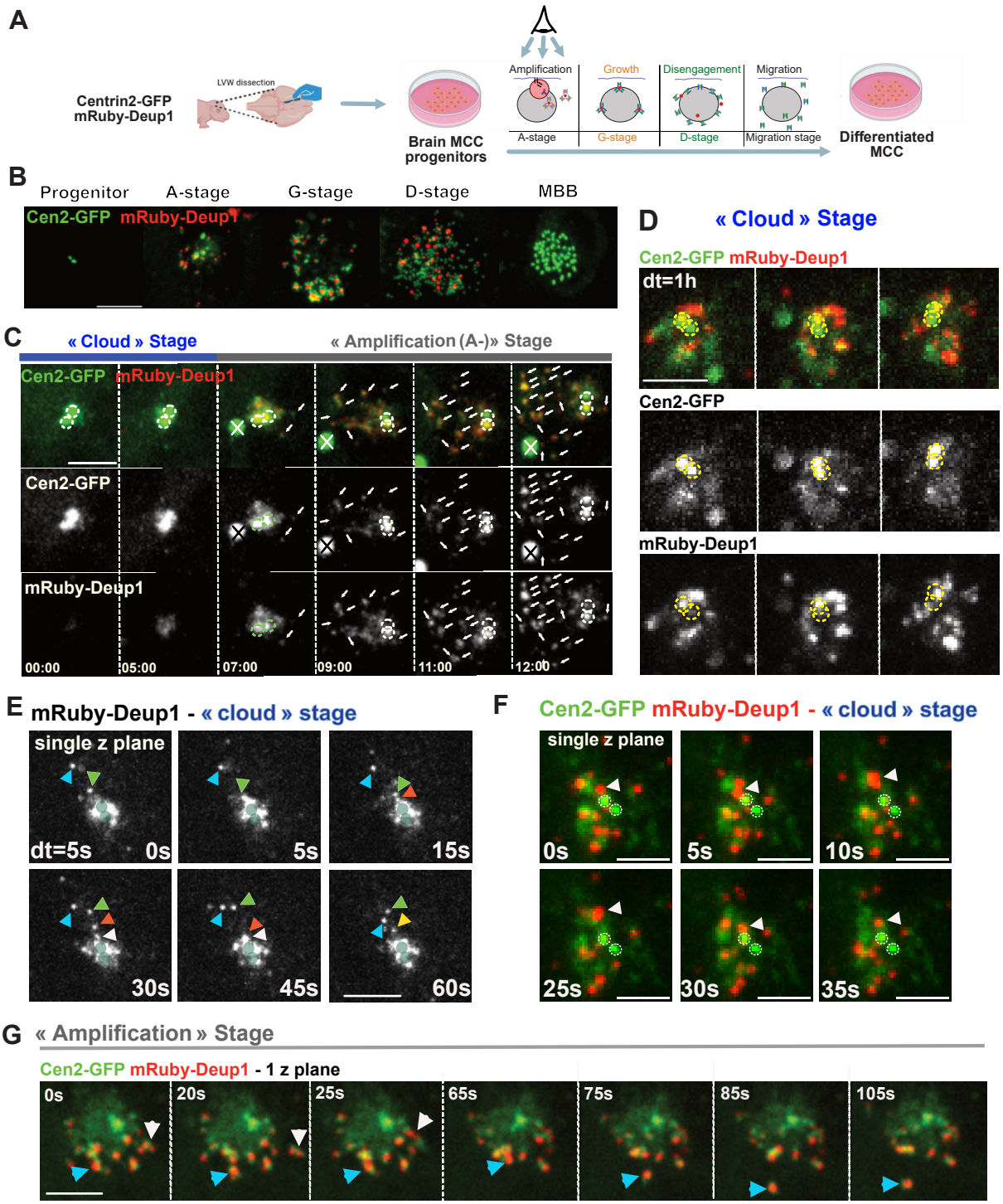
A
Centrin2-GFP
mRuby-Deup1
LVW dissection
Brain MCC progenitors
Amplification
Growth
Disengagement
Migration
A-stage
G-stage
D-stage
Migration stage
Differentiated MCC
B
Progenitor
A-stage
G-stage
D-stage
MBB
Cen2-GFP mRuby-Deup1
C
« Cloud » Stage
« Amplification (A-)» Stage
Cen2-GFP mRuby-Deup1
Cen2-GFP
mRuby-Deup1
00:00
05:00
07:00
09:00
11:00
12:00
D
« Cloud » Stage
Cen2-GFP mRuby-Deup1
dt=1h
Cen2-GFP
mRuby-Deup1
E
mRuby-Deup1 - « cloud » stage
single z plane
dt=5s
0s
5s
15s
30s
45s
60s
F
Cen2-GFP mRuby-Deup1 - « cloud » stage
single z plane
0s
5s
10s
25s
30s
35s
G
« Amplification » Stage
Cen2-GFP mRuby-Deup1 - 1 z plane
0s
20s
25s
65s
75s
85s
105s

# Figure 3

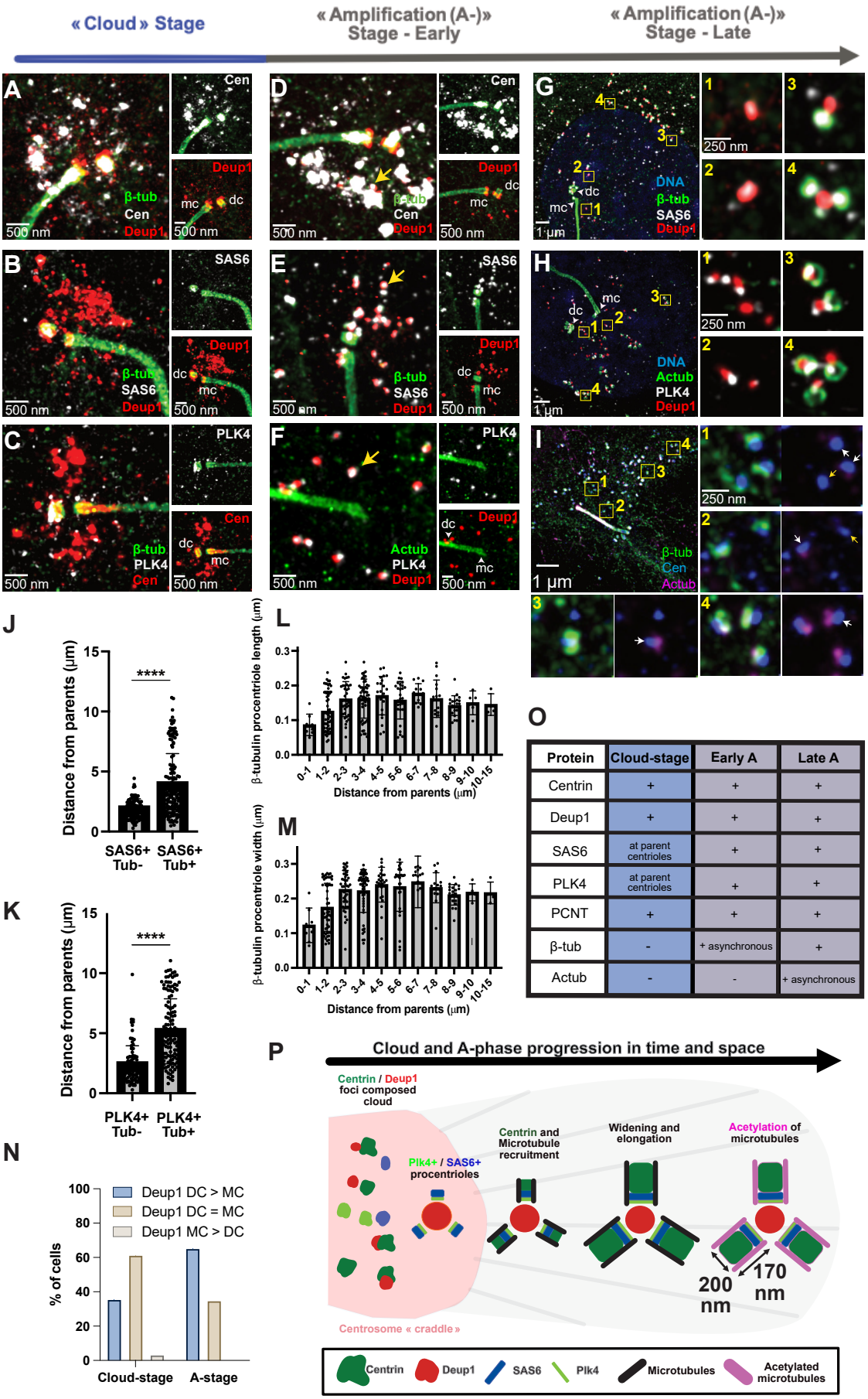


O

| Protein | Cloud-stage | Early A | Late A |
|---|---|---|---|
| Centrin | + | + | + |
| Deup1 | + | + | + |
| SAS6 | at parent centrioles | + | + |
| PLK4 | at parent centrioles | + | + |
| PCNT | + | + | + |
| β-tub | - | + asynchronous | + |
| Actub | - | - | + asynchronous |

# Figure 4

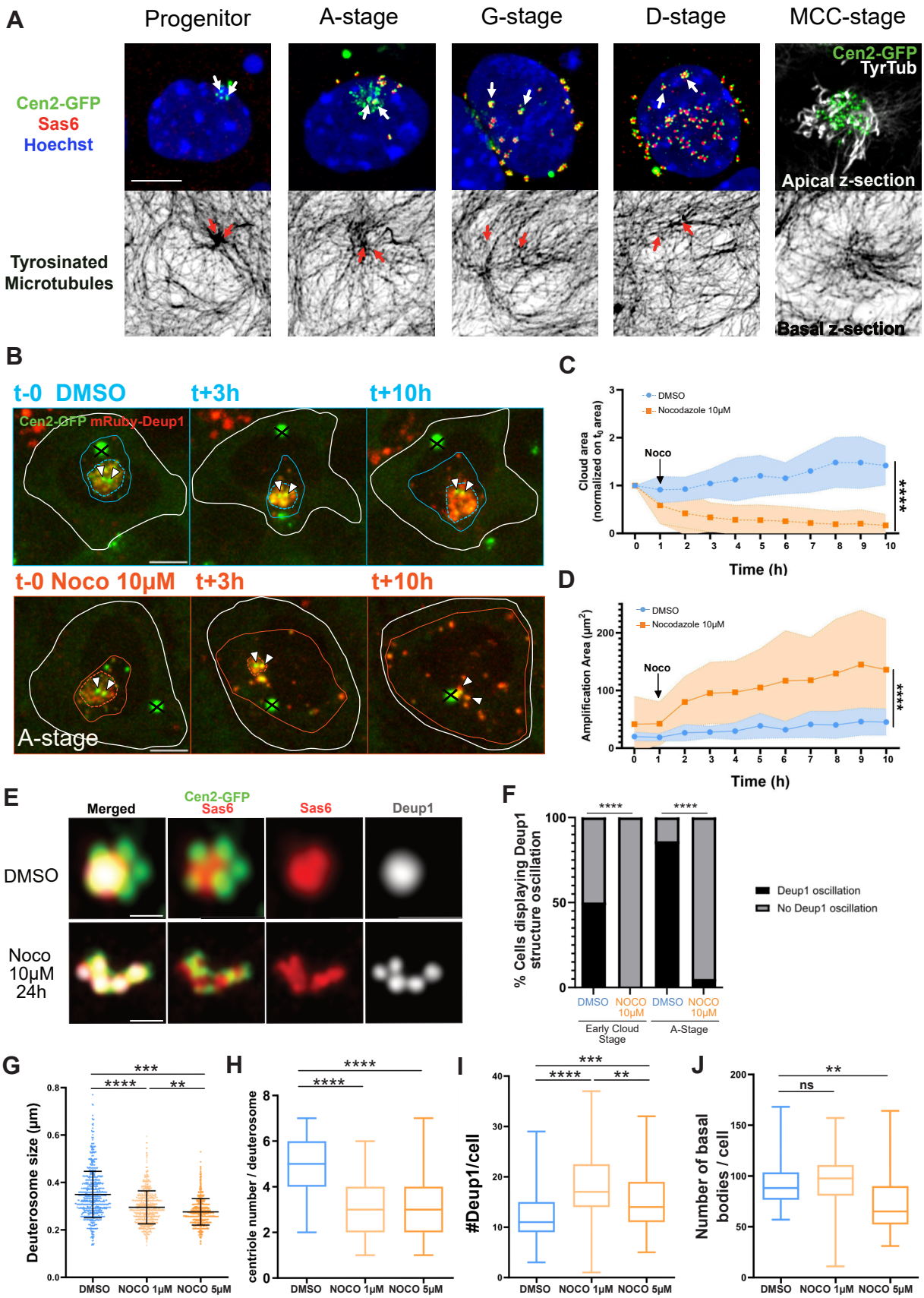
A
Progenitor
A-stage
G-stage
D-stage
MCC-stage
Cen2-GFP
Sas6
Hoechst
Tyrosinated Microtubules
Cen2-GFP
TyrTub
Apical z-section
Basal z-section
B
t-0 DMSO
t+3h
t+10h
Cen2-GFP mRuby-Deup1
t-0 Noco 10µM
t+3h
t+10h
A-stage
C
DMSO
Nocodazole 10µM
Noco
Cloud area (normalized on t0 area)
Time (h)
****
D
DMSO
Nocodazole 10µM
Noco
Amplification Area (µm²)
Time (h)
****
E
Merged
Cen2-GFP Sas6
Sas6
Deup1
DMSO
Noco 10µM 24h
F
% Cells displaying Deup1 structure oscillation
****
****
DMSO
NOCO 10µM
DMSO
NOCO 10µM
Early Cloud Stage
A-Stage
Deup1 oscillation
No Deup1 oscillation
G
Deuterosome size (µm)
***
****
**
DMSO
NOCO 1µM
NOCO 5µM
H
centriole number / deuterosome
****
****
DMSO
NOCO 1µM
NOCO 5µM
I
#Deup1/cell
***
****
**
DMSO
NOCO 1µM
NOCO 5µM
J
Number of basal bodies / cell
**
ns
DMSO
NOCO 1µM
NOCO 5µM

# Figure 5

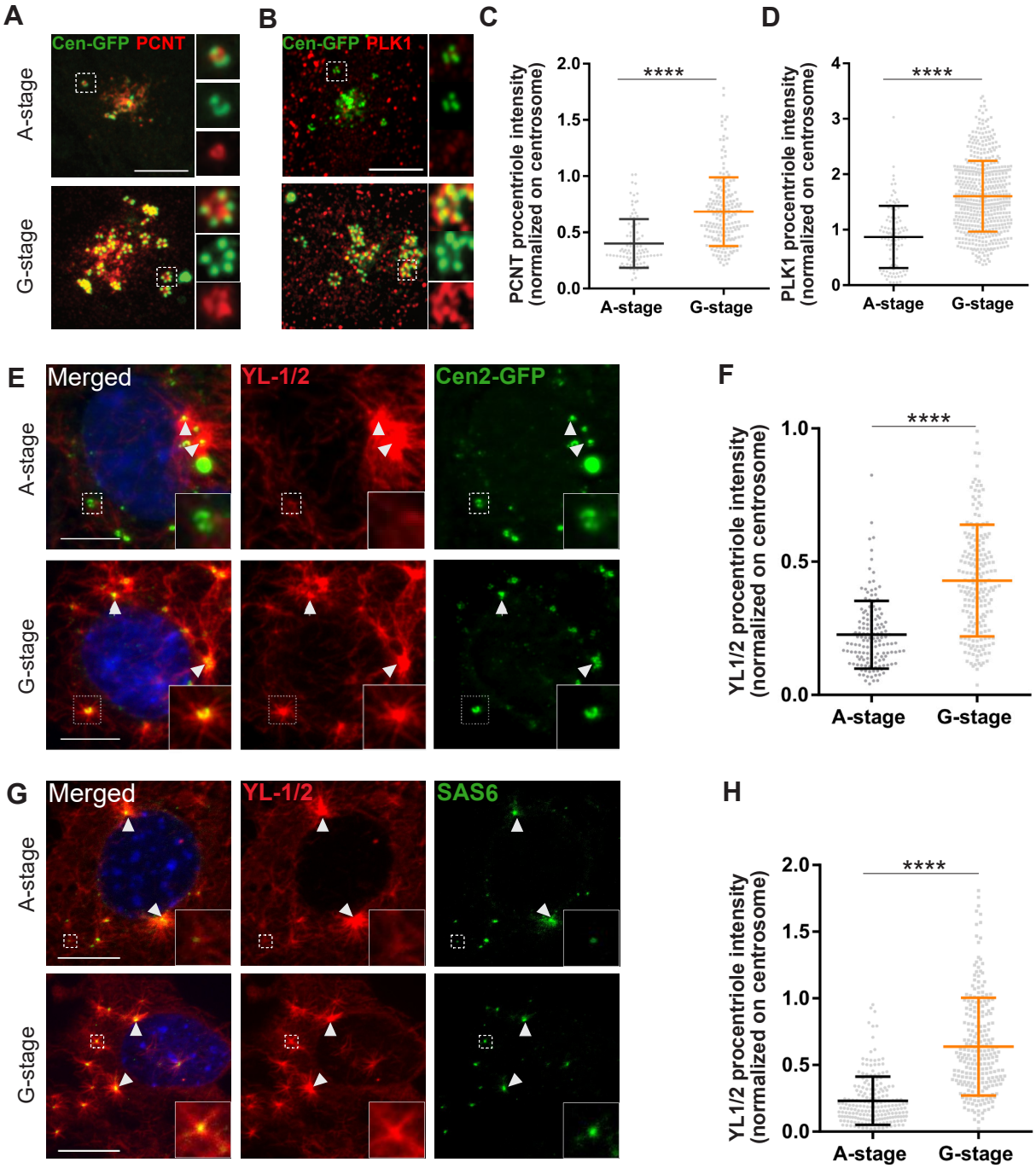
A
Cen-GFP PCNT
A-stage
G-stage
B
Cen-GFP PLK1
C
PCNT procentriole intensity (normalized on centrosome)
2.0
1.5
1.0
0.5
0.0
****
A-stage
G-stage
D
PLK1 procentriole intensity (normalized on centrosome)
4
3
2
1
0
****
A-stage
G-stage
E
Merged
YL-1/2
Cen2-GFP
A-stage
G-stage
F
YL1/2 procentriole intensity (normalized on centrosome)
1.0
0.5
0.0
****
A-stage
G-stage
G
Merged
YL-1/2
SAS6
A-stage
G-stage
H
YL1/2 procentriole intensity (normalized on centrosome)
2.0
1.5
1.0
0.5
0.0
****
A-stage
G-stage

# Figure 6

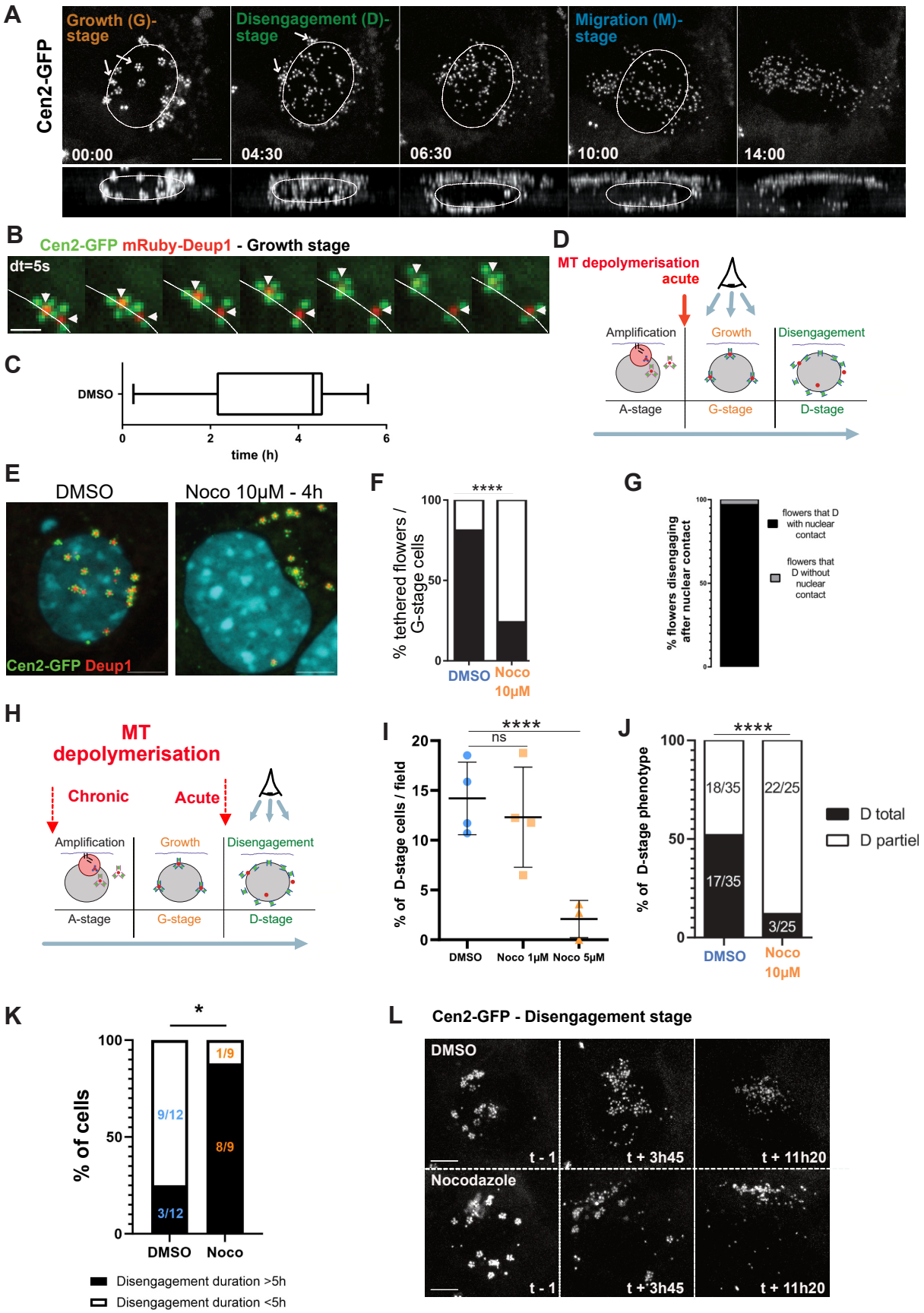
A
Cen2-GFP
Growth (G)-stage
Disengagement (D)-stage
Migration (M)-stage
00:00
04:30
06:30
10:00
14:00
B
Cen2-GFP mRuby-Deup1 - Growth stage
dt=5s
C
DMSO
0
2
4
6
time (h)
D
MT depolymerisation acute
Amplification
Growth
Disengagement
A-stage
G-stage
D-stage
E
DMSO
Noco 10µM - 4h
Cen2-GFP Deup1
F
****
% tethered flowers / G-stage cells
100
50
0
DMSO
Noco 10µM
G
% flowers disengaging after nuclear contact
flowers that D with nuclear contact
flowers that D without nuclear contact
H
MT depolymerisation
Chronic
Acute
Amplification
Growth
Disengagement
A-stage
G-stage
D-stage
I
****
ns
% of D-stage cells / field
20
15
10
5
0
DMSO
Noco 1µM
Noco 5µM
J
****
% of D-stage phenotype
100
50
0
18/35
17/35
22/25
3/25
DMSO
Noco 10µM
D total
D partiel
K
*
% of cells
100
50
0
9/12
3/12
1/9
8/9
DMSO
Noco
Disengagement duration >5h
Disengagement duration <5h
L
Cen2-GFP - Disengagement stage
DMSO
Nocodazole
t - 1
t + 3h45
t + 11h20

# Figure 7

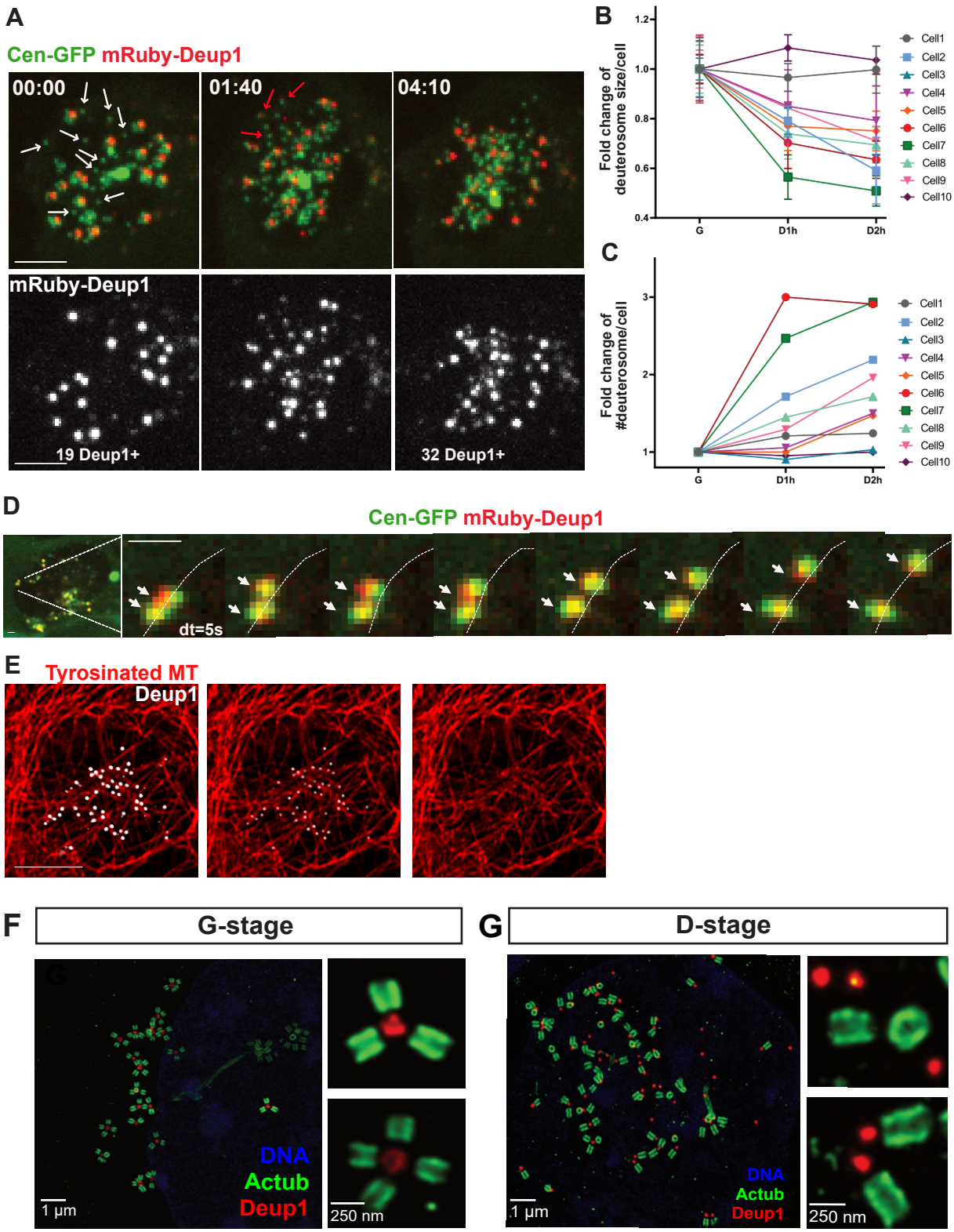
A
Cen-GFP mRuby-Deup1
00:00
01:40
04:10
mRuby-Deup1
19 Deup1+
32 Deup1+
B
Fold change of deuterosome size/cell
1.2
1.0
0.8
0.6
0.4
G
D1h
D2h
Cell1
Cell2
Cell3
Cell4
Cell5
Cell6
Cell7
Cell8
Cell9
Cell10
C
Fold change of #deuterosome/cell
3
2
1
G
D1h
D2h
Cell1
Cell2
Cell3
Cell4
Cell5
Cell6
Cell7
Cell8
Cell9
Cell10
D
Cen-GFP mRuby-Deup1
dt=5s
E
Tyrosinated MT
Deup1
F
G-stage
DNA
Actub
Deup1
1 µm
250 nm
G
D-stage
DNA
Actub
Deup1
1 µm
250 nm

# Figure 8

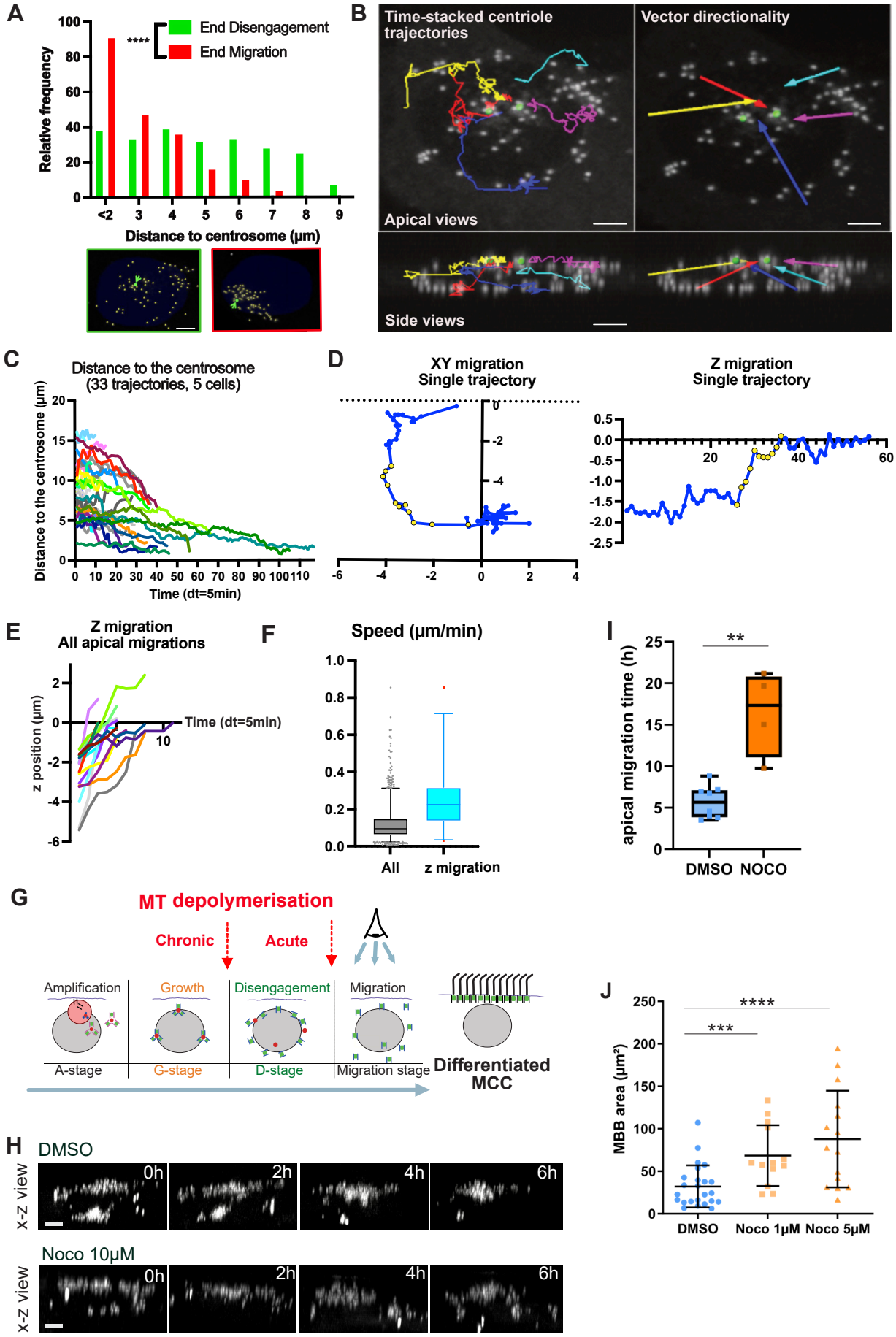
A
Relative frequency
End Disengagement
End Migration
****
Distance to centrosome (µm)
B
Time-stacked centriole trajectories
Vector directionality
Apical views
Side views
C
Distance to the centrosome (33 trajectories, 5 cells)
Distance to the centrosome (µm)
Time (dt=5min)
D
XY migration Single trajectory
Z migration Single trajectory
E
Z migration All apical migrations
z position (µm)
Time (dt=5min)
F
Speed (µm/min)
All
z migration
I
apical migration time (h)
**
DMSO
NOCO
G
MT depolymerisation
Chronic
Acute
Amplification
Growth
Disengagement
Migration
A-stage
G-stage
D-stage
Migration stage
Differentiated MCC
J
MBB area (µm²)
****
***
DMSO
Noco 1µM
Noco 5µM
H
DMSO
Noco 10µM
x-z view
0h
2h
4h
6h

Figure 9

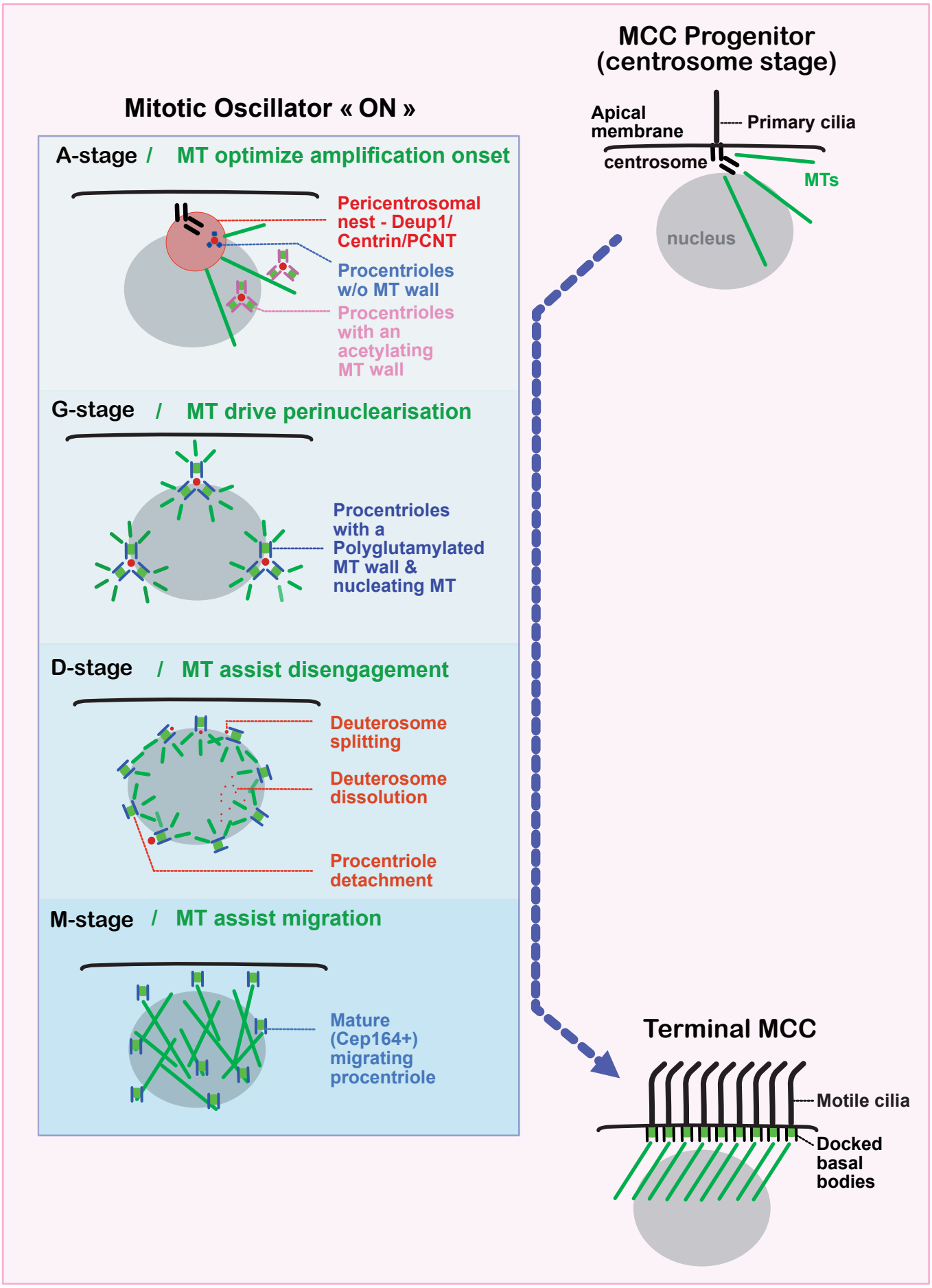
MCC Progenitor
(centrosome stage)
Apical membrane
Primary cilia
centrosome
MTs
nucleus
Mitotic Oscillator « ON »
A-stage / MT optimize amplification onset
Pericentrosomal nest - Deup1/ Centrin/PCNT
Procentrioles w/o MT wall
Procentrioles with an acetylating MT wall
G-stage / MT drive perinuclearisation
Procentrioles with a Polyglutamylated MT wall & nucleating MT
D-stage / MT assist disengagement
Deuterosome splitting
Deuterosome dissolution
Procentriole detachment
M-stage / MT assist migration
Mature (Cep164+) migrating procentriole
Terminal MCC
Motile cilia
Docked basal bodies